Built on LDRD Laboratory Directed Research and Development

SAND20XX-XXXXR
LDRD PROJECT NUMBER: 209697
LDRD PROJECT TITLE: ChemoMechanical Controls on Induced Seismicity
PROJECT TEAM MEMBERS: R. Charles Choens, Anastasia Ilgen, Carlos Jove-Colon, Jennifer Wilson, Moo Lee

ABSTRACT:

In recent years, seismicity rates in the US have dramatically risen due to increased activity in onshore oil and gas production. This project attempts to tie observations about induced seismicity to dehydration reactions in laumontite, a common mineral found in fault gouge in crystalline basement formations. It is the hypothesis of this study that in addition to pressure-related changes in the in situ stress state, the injection of wastewater pushes new fluids into crystalline fault fracture networks that are not in chemical equilibrium with the mineral assemblages, particularly laumontite in fault gouge. Experiments were conducted under hydrothermal conditions where samples of laumontite were exposed to NaCl brines at different pH values. After exposure to different fluid chemistries for 8 weeks at 90° C, we did not observe substantial alteration of laumontite. In hydrostatic compaction experiments, all samples deformed similarly in the presence of different fluids. Pore pressure decreases were observed at the start of a 1 week hold at 85° C in a 1M NaCl pH 3 solution, suggesting that acidic fluids might stabilize pore pressures in basement fault networks. Friction experiments on laumontite and kaolinite powders showed both materials have similar coefficients of friction. Mixtures with partial kaolinite content showed a slight decrease in the coefficient of friction, which could be sufficient to trigger slip on critically stressed basement faults.

INTRODUCTION:

Since 2009, the seismicity rate in the midcontinent US has increased by three orders of magnitude, posing a large threat to the region [*Ellsworth*, 2013; *Keranen et al.*, 2013; *Keranen et al.*, 2014]. The increase in seismicity has been tied to high volume disposal wells, that inject flowback and produced water from oil and gas wells, as well as a handful of events linked to hydraulic fracturing [*Friberg et al.*, 2014; *Keranen et al.*, 2013; *Keranen et al.*, 2014; *Skoumal et al.*, 2015]. Earthquakes are concentrated in Oklahoma, but seismicity associated with unconventional resources has been observed in Ohio, Kansas, Colorado, Arkansas, California, Texas, and the UK [*Clarke et al.*, 2014; *Ellsworth*, 2013; *Goebel et al.*, 2016; *Kim*, 2013; *McMahon et al.*, 2017; *McNamara et al.*, 2015; *Van der Elst et al.*, 2013]. Observed events are anywhere from magnitudes of -2 to 5.8, large enough to cause structural damage. Magnitude 5+ events have occurred within kilometers of Cushing, Oklahoma, a major crude oil pipeline and

Sandia National Laboratories is a multimission laboratory managed and operated by National Technology and Engineering Solutions of Sandia, LLC, a wholly owned subsidiary of Honeywell International, Inc., for the U.S. Department of Energy's National Nuclear Security Administration under contract DE-NA-0003525.

storage hub [*Holland*, 2013; *McMahon et al.*, 2017; *Norbeck and Rubinstein*, 2018]. The earthquakes are believed to be triggered by elevated fluid pressures from injection wells as large volumes of fluids have been injected at high pressures into formations overlying the crystalline basement [*Helmold and van de Kamp*, 1984; *Holland*, 2013; *McNamara et al.*, 2015]. Injected fluid volumes are sufficient to create 3 mm/year surface uplift up to 8 km away from high volume injection wells [*Shirzaei et al.*, 2016]. In many cases, seismicity can be delayed by decades from the onset of injections, large volumes of fluids can be injected without affecting seismicity, and seismicity rates can remain elevated even after injection stops [*Goebel et al.*, 2017; *Norbeck and Rubinstein*, 2018]. Studies have shown that hypocenters from the induced events are 2-8 km deep, located on preexisting fault systems in the crystalline basement beneath sedimentary basins [*Friberg et al.*, 2014; *Holland*, 2013; *Keranen et al.*, 2013; *Kim*, 2013; *McMahon et al.*, 2017; *McNamara et al.*, 2015; *Skoumal et al.*, 2015]. Some events occur in sedimentary cover, but the vast majority of energy released is from slip on basement faults [*McMahon et al.*, 2017]. The injected fluids increase pore pressure in basement fault and fracture networks, allowing them to slip under current in situ stresses. Geologic factors have been identified that control the location of induced seismicity. Thick sedimentary covers (>4km) lack injection related seismicity as more permeable sedimentary formations diffuse injected fluids before they can pressurize basal faults [*Shah and Keller*, 2017]. Basement lithology is also important, as undeformed extrusive basement formations do not display the elevated seismic activity like faulted and fractured intrusive and metamorphic basement formations [*Shah and Keller*, 2017].

Disposal wells have been linked to seismic activity on basement faults as far back as the 1960's with induced earthquake swarms at the Rock Mountain Arsenal [*D M Evans*, 1966; *Healy et al.*, 1968]. Within 6 years, large events had migrated 10 km from the injection point. Events tracked injection rates and decayed after injection stopped. Seismicity continued for two decades after injection ceased, cumulating in a magnitude 4.3 event that occurred in 1981 [*Ellsworth*, 2013]. Scientific drilling projects and enhanced geothermal projects have also demonstrated seismicity associated with elevated fluid pressures in crystalline basement fault and fracture networks [*Erzinger and Stober*, 2005; *Häring et al.*, 2008; *Jahr et al.*, 2008; *Meller and Ledésert*, 2017; *Shapiro et al.*, 2006; *Stober and Bucher*, 2005; 2015]. At the German Deep Drilling Site, KTB, a 9 km deep well was drilled into the crystalline basement that intersected two dominant fault systems at 4 km and 7.2 km depth. Long term hydraulic experiments were conducted to investigate induced seismicity on a continental scale fault system from 2002-2005 [*Stober and Bucher*, 2005]. For the first year, 22,300 m^3 of fluids were produced from the 4 km deep fault network, during which seismicity was absent [*Stober and Bucher*, 2015]. Over the next ten months, 84,600 m^3 of water was injected back into the 4 km deep fault network [*Stober and Bucher*, 2005]. Pore pressure in the fault system changed by as much as 10 MPa, resulting in 3.1 mm of uplift observed above the injection point due to induced deformation [*Jahr et al.*,

2008]. Seismicity began when the injected volume roughly equaled the withdrawn volume [*Shapiro et al.*, 2006]. According to diffusivity estimates of the fault network, elevated pore pressures of 0.001 – 0.1 MPa were present at induced hypocenters [*Shapiro et al.*, 2006]. These observations demonstrate that basement faults are highly sensitive to small pore pressure increases, and that fault-fracture networks form high permeability hydraulic pathways capable of advective transport in otherwise impermeable formations [*Shapiro et al.*, 2006]. At the St. Gallen deep geothermal project in Switzerland, seismicity initiated within 80 minutes of hydraulic stimulation tests. The geothermal project was targeting permeable fault and fracture networks, but hydraulic connections to deeper faults allowed for the reactivation of critically stressed faults below the borehole and target intervals [*Diehl et al.*, 2017]. Similarly, seismic activity has been observed associated with stimulation projects at the Soultz-sous-Forets in Alsace, France. Hundreds of micro-earthquakes were recorded during stimulation tests, but the largest events occurred after shut-in [*Horálek et al.*, 2010]. Seismic source analysis of magnitude 1.4+ events indicate slip on pre-existing faults as opposed to hydraulic fracturing [*Horálek et al.*, 2010]. Locations of seismic events are partially controlled by mineralogy [*Meller and Ledésert*, 2017]. Clay filled fracture intervals had lower magnitude seismicity compared to clay free fracture intervals, likely due to reduced frictional strength of clays and their tendency towards aseismic deformation. Clay rich intervals were associated with high calcite anomalies, suggesting that alteration formed due to late circulations of fluids enriched in Ca^{++} and CO_2. Organic matter observed in fractures suggests a connection to surface waters [*Meller and Ledésert*, 2017].

Observations of fault and fracture networks in exposed crystalline basement formations demonstrate that faults and fractures that formed at depth are filled with hydrothermal alteration products. Because faults and fractures are highly permeable and crystalline formations are not, alteration is concentrated on fracture surfaces [*Meller and Ledésert*, 2017]. The type of alteration product depends on the temperature and fluid history of the fault system. In situ brines in basement formations often represent relic seawater trapped in the formation [*Bucher and Stober*, 2010]. These brines are impacted by long-term fluid-rock interactions, and as a result can have neutral to high pH, little to no dissolved CO_2, and high levels of dissolved solids like chlorides, sulfates, and bicarbonates [*Bucher and Stober*, 2010; *Erzinger and Stober*, 2005; *Gascoyne and Kamineni*, 1994; *Stober and Bucher*, 2015]. In the upper continental crust (temperature <250° C) secondary Ca-Al silicates like epidote, prehnite, and zeolite are predicted alteration products between granites and brines [*Mironenko and Zolotov*, 2012; *Savage*, 1986]. The zeolite laumontite is one of the most common alteration products of plagioclase feldspar, a major constituent of granite and gneisses that make up the crystalline basement and continental crust [*Savage*, 1986; *Trotignon et al.*, 1999; *Weisenberger and Bucher*, 2010]. In basement formations with hydraulic connections to the shallower aquifers and meteoric derived fluids, dissolved solids levels are lower, pH is lower, and CO_2 activity is higher. In these systems,

fractures are filled with clay minerals like montmorillonite, kaolinite, illite, and smectite [*Schleicher et al.*, 2006; *Zwingmann and Mancktelow*, 2004]. In northeastern Oklahoma, seismicity correlates to different basement geology [*Shah and Keller*, 2017]. Seismicity is absent where the basement is composed of undeformed extrusive rocks, mafic intrusions, and the Osage microgranite, a small granite batholith devoid of plagioclase [*Denison*, 1981]. Earthquakes occur within highly deformed, plagioclase-rich granites and granitoids of the Central Oklahoma granite group, the inferred Midcontinental rift, and the western part of the Spavinaw granite [*Denison*, 1981; *Shah and Keller*, 2017]. Observations of fault and fracture systems in granites suggest that the Oklahoma basement faults should be permeable hydraulic conduits, susceptible to reactivations, and at P-T conditions to form hydrothermal reaction products in fractures.

Laumontite is a framework aluminosilicate mineral composed of rings of $SiAlO_4$ tetrahedra. These rings link to form a cage like structure that create cavities and channels that allow for easy transport and/or exchange of ions. Bonded water is loosely attached to the interior of the cage structure and can be easily removed or replaced without affecting the framework bonds [*Gottardi and Galli*, 1985]. Laumontite has been observed as fracture fill in freshly exposed granites in the Alps, but it has also been observed in several characteristic locations [*Chipera and Apps*, 2001; *Hay*, 1966; *Weisenberger and Bucher*, 2010]. It is associated with large scale faults in California in the San Andreas fault system [*Helmold and van de Kamp*, 1984; *Schleicher et al.*, 2009; *Solum et al.*, 2006; *Vincent and Ehlig*, 1988]. It has been observed in the San Gabriel and Punchbowl fault cores that were active at depths of 2-5 km; heavily altered portions of the San Gabriel fault have several generations of laumontite veins [*J P Evans and Chester*, 1995]. Laumontite veins have also been observed in the Cajon Pass formation that likely formed at 2.5-3.5 km burial depth [*Vincent and Ehlig*, 1988]. Laumontite is not observed in shallower formations, indicating that alteration could have been caused by upwelling of hot fluids at depth that would have been sealed by a lacustrine member of the Cajon Pass formation [*Vincent and Ehlig*, 1988]. Laumontite was also found at depth along the San Andreas fault [*Schleicher et al.*, 2009; *Solum et al.*, 2006]. It is present both in the formations along the fault and in fault gouges formed in situ in the active trace of the fault. In the Western Transverse Ranges, California, deeper fluids upwell at the surface in a series of hot springs, creating unique conditions that allow laumontite to form above ground at the Sespe Hot Springs [*McCulloh et al.*, 1981].

Laumontite is formed during albitization of plagioclase feldspar at temperatures from ~75-250° C [*Crossey et al.*, 1984; *Helmold and van de Kamp*, 1984; *Ivanov and Gurevich*, 1975]:

$$NaAlSi_3O_8 \cdot CaAl_2Si_2O_8 + 2SiO_2 + 4H_2O \rightarrow NaAlSi_3O_8 + CaAl_2Si_4O_{12} \cdot 4H_2O \quad (1)$$
$$Plagioclase + Quartz + Water \rightarrow Albite + Laumontite.$$

In the presence of pore fluids with high CO_2 activity, laumontite dehydrates to form calcite and kaolinite:

$$CaAl_2Si_4O_{12} \cdot 4H_2O + CO_2 \rightarrow CaCO_3 + Al_2Si_2O_5(OH)_4 + 2SiO_2 + 2H_2O \quad 2)$$
$$Laumontite + Carbon\ Dioxide \rightarrow Calcite + Kaolinite + Quartz + Water.$$

In low pH fluids, laumontite will also dehydrate to form kaolinite:

$$CaAl_2Si_4O_{12} \cdot 4H_2O + 2H^+ \rightarrow Al_2Si_2O_5(OH)_4 + 2SiO_2 + Ca^{2+} + 3H_2O \quad 3)$$
$$Laumontite + Hydrogen\ ions \rightarrow Kaolinite + Quartz + Calcium + Water.$$

Reaction 2 results in a volume decrease of 10%, and reaction 3 results in a volume decrease of 28% [*Crossey et al.*, 1984]. Excess water is also generated during these reactions, which could create an increase in pore pressure depending on the kinetics of the reaction. The higher temperature dehydration reaction of laumontite to wairakite has been studied, and this reaction generates excess pore pressure that could trigger seismicity [*Hacker*, 1997; *Jove and Hacker*, 1997; *Liou*, 1971]. The lower temperature dehydration reaction to kaolinite has limited investigations [*Savage et al.*, 1993]. Dissolution experiments on laumontite have demonstrated that dissolution is non-stoichiometric and surface controlled [*Voltolini et al.*, 2012]. CO_2 percolation experiments in laumontite cemented sandstones have demonstrated that this dehydration reaction can occur quickly (1-week experiments), and it can affect hydraulic properties. Kaolinite precipitated along laumontite grain surfaces and fracture walls, clogging pore throats and reducing permeability [*Luquot et al.*, 2012].

The mineralogical composition and mechanical behavior of fault gouge in major active faults has been the focus of many investigations to understand its influence on fault seismicity and creep deformation [*Lockner et al.*, 2011; *Moore and Lockner*, 2007; *Moore and Rymer*, 2007; *Morrow et al.*, 2017; *Saffer et al.*, 2012; *Solum et al.*, 2006; *Tembe et al.*, 2010]. The influence of mineral dehydration and the build-up of fluid pressure has also been proposed as a potential mechanism in weak fault behavior and induced seismicity [*Hacker*, 1997; *Jove and Hacker*, 1997]. Others have proposed that the inherent occurrence of "weak" minerals in fault gouge is the main control to the fault's weak behavior as observed in some segments of the San Andreas Fault (SAF) [*Zoback*, 2010]. Pressure-temperature stability relations of hydrous clay and zeolite minerals could play an important role in the fault frictional behavior. Moreover, the stability of these minerals is also controlled by the local fluid chemistry interacting with these phases and gouge material [*Blanpied et al.*, 1998; *J P Evans and Chester*, 1995; *Jove and Hacker*, 1997; *Moore and Rymer*, 2007; *Morrow et al.*, 2000]. Therefore, the application of thermodynamic analysis to fluid-mineral equilibria can be useful in the evaluation of phase stability at various conditions of pressure, temperature, and fluid composition. In this report, we focus this analysis on the equilibria between laumontite (lmt) ($CaAl_2Si_4O_{12}$•$4H_2O$), partially-dehydrated laumontite or "leonhardite" ("leonh"), and kaolinite (kaol). We also evaluate stability relations in the absence and presence of CO_2 to assess the relative stability of calcite with respect

to Ca-bearing solutions. It should be noted that the mineral name "leonhardite" has been discredited by the International Mineralogical Association, Subcommittee on Zeolites [*Coombs et al.*, 1997], and it's used here in quotes referring to partially-dehydrated laumontite. Laumontite is a common zeolite facies mineral found in fracture fillings as a result of the alteration of volcanic material and Ca-bearing feldspar [*Jove and Hacker*, 1997]. This mineral is ideal to study dehydration reactions given its simple mechanism of dehydration with temperature.

Dehydration reactions can create complicated interactions between fault slip, fracturing, and chemical reactions. Serpentinite is predicted to begin dehydration reactions at the depths where seismicity occurs along subduction zones [*Brantut et al.*, 2011; *Hacker*, 1997; *Okazaki and Hirth*, 2016], and the dehydration of gypsum is a low temperature analog for serpentinite reactions [*Ko et al.*, 1995; *Wong et al.*, 1997]. Studies have demonstrated that dehydration can release substantial pore fluids, in excess of 100 MPa and volume strains over 20% [*Ko et al.*, 1997; *Llana□Fúnez et al.*, 2007]. The reaction can also induce a fracture network, changing the microstructure of the rock. As the reaction initiates, pore pressure increase and generate fractures[*Ko et al.*, 1997; *Olgaard et al.*, 1995]. Coalescence of these fractures create permeable networks that drain excess pore fluids [*French and Zhu*, 2017; *Leclère et al.*, 2016; *Milsch and Priegnitz*, 2012]. High pore pressures inhibit the dehydration reaction, so the permeable channels create positive feedback to complete the dehydration reactions [*Malvoisin et al.*, 2017]. In experiments, reactions initiate at drained ends of samples along slip planes in friction experiments [*Leclère et al.*, 2016; *Miller et al.*, 2003; *Milsch and Priegnitz*, 2012]. Generation of pore pressures lowers normal stress and triggers slip.

Induced seismicity is associated with high volume injection wells disposing of used hydraulic fracturing fluid and produced waters from unconventional reservoirs into formation directly overlying the basement. Injected wastewater differs from basement fluids in two critical ways: injected fluids tend to have low to neutral pH and moderate to high levels of CO_2 [*Gregory et al.*, 2011; *Ramudo and Murphy*, 2010]. Fluids are treated with mild acids to dissolve carbonate minerals in fractures and prevent the development of scale [*Gregory et al.*, 2011]. After stimulation, fluids are flown back and are further altered by interactions with the shale reservoirs. Production of oil and gas from shales also creates high volumes of produced waters for disposal. Studies have shown that fluids become increasing acidic with production [*Barbot et al.*, 2013; *Lester et al.*, 2015].

Observations of crystalline basement demonstrate that fault-fracture systems are permeable networks capable of advective transport [*Stober and Bucher*, 2015]. Injecting large volumes of fluids into sedimentary formations in hydraulic connectivity with basement faults would push new fluids along these networks, changing the fluid-rock equilibrium. The fractures are filled with hydrothermal alteration products like laumontite, which is unstable in the presence of fluids with low pH or high CO_2 contents [*Helmold and van de Kamp*, 1984; *Luquot et al.*,

2012]. This dehydration reaction could affect seismicity in several ways: the reaction products have lower coefficient of frictions than laumontite, lowering the shear strength of the fault; generation of excess pore fluids could raise pore pressures to trigger slip; volume decreases of the dehydration reaction could increase pore volume and inhibit slip; precipitation of kaolinite at pore throats could reduce permeability and create local spikes in pore pressure; or higher pore volumes could increase permeability to diffuse pore pressure spike [*Bernaudin and Gueydan*, 2018; *Miller et al.*, 2003; *Moore and Lockner*, 2013; *Morrow et al.*, 2000; *Scuderi et al.*, 2017; *Tembe et al.*, 2010]. In this study, we conducted experiments on laumontite under different pH fluids to determine the kinetics of its dehydration reaction and resulting mechanical response to assess its potential impact on induced seismicity.

DETAILED DESCRIPTION OF EXPERIMENT:

Thermodynamic modelling

Analysis of stability relations requires retrieval of thermodynamic data for the phases of interest. Thermodynamic data for laumontite and "leonhardite" was obtained from the analysis of *Neuhoff and Bird* [2001]. Data for kaolinite is from the THERMODDEM database [*Blanc et al.*, 2012]. Thermodynamic analysis of chemical reactions and generation of activity phase diagrams was conducted using the CHNOSZ software [*Dick*, 2008]. This open source software (developed in R language) includes multiple functions and data to conduct chemical thermodynamic modeling covering large sets of chemical species for biochemistry and geochemistry. It also accepts standard thermodynamic data parameters for mineral, aqueous species, and gases like the SUPCRT92 computer code. Thermodynamic data tabulated by *Neuhoff and Bird* [2001] was added to the CHNOSZ mineral database along with heat capacity coefficients for extrapolations as a function of temperature. The phase transition of laumontite to "leonhardite" was constrained after the analysis of *Neuhoff and Bird* [2001] based on calorimetric measurements.

Material

The laumontite used in this study was collected from outcrops in California obtained from commercially available sources. Two different grain size fractions were used in this study: a fine powder (pharmaceutical grade laumontite) and a granular sand. Fine grained powders were used in chemical kinetics experiments, and granular samples were used in chemical kinetics experiments and compaction experiments. Friction experiments were performed with fine grained laumontites mixed with kaolinite powders to simulate different stages of completion for dehydration reactions.

To separate laumontite from the mineral mixture received, we used density separation. This method allows for mineral separation from their mixture: minerals are suspended in a dense

fluid, resulting in lighter mineral components floating, and heavier components sinking. Sodium polytungstate solution (NaPT) was diluted to the target density of 2.5 g/mL. Mineral mixture of fine-grain laumontite was suspended and either centrifuged, or allowed to separate overnight by settling. The lighter fraction (floating fraction) was collected and washed with de-ionized H_2O. Since laumontite was the lightest mineral among the identified components, our expectation was that it would be enriched in this separated fraction.

Solid-phase analysis.

To identify crystalline phases in the received laumontite materials and in altered mineral mixtures, randomly oriented dried sample powders were analyzed by powder X-ray diffraction (XRD). We used a D2 Phaser Research Diffractometer (Bruker) equipped with a Cu (Kα λ = 1.54277 Å) X-ray tube with the generator set at 30 kV and 10 mA. Scans were collected from 5 to 75 degrees 2θ and a counting time of 1 second per point at 0.1-degree step size. Search/match protocol was used to identify mineral phases, with ICDD 2017 crystal structure database. The proportions of different minerals in the samples were determined using semi-quantitative XRD analysis via relative peak intensities routine embedded within the Eva software (Bruker).

Alteration experiments.

Seven alteration experiments were run to quantify mineralogical transformations that laumontite mineral mixtures undergo at different pH values, with and without carbon dioxide (CO_2). These alteration reactors included:

1. Powdered laumontite in de-ionized H_2O
2. Powdered laumontite in 1M NaCl at pH 3
3. Powdered laumontite in 1M NaCl at pH 6
4. Powdered laumontite in 1M NaCl, initially at pH 6 with CO_2
5. Granular (< 0.425 mm) laumontite in 1M NaCl at pH 3
6. Granular (< 0.425 mm) laumontite in 1M NaCl at pH 6
7. Granular (< 0.425 mm) laumontite in 1M NaCl, initially at pH 6 with CO_2

Two grams of mineral mixtures were loaded into Parr reactors, then 50 mL of either de-ionized water or 1M NaCl were added. Carbon dioxide, in the form of dry ice, was added in the amount of 40 grams to the reactors #4 and #7. Reactors were set in an oven at 90 °C for 8 weeks. The reactors were inverted daily to allow mixing of their content. When alteration experiment was completed, reactors were cooled to room temperature, and then solid and aqueous phases were separated. Aqueous phase was filtered using 0.45 µm nylon membrane filter, and preserved by the addition of 6N ultrapure HNO_3.

Aqueous phase analysis.

Concentrations of dissolved calcium (Ca), magnesium (Mg), potassium (K), strontium (Sr), silicon (Si), aluminum (Al), and iron (Fe) were quantified using inductively coupled plasma

mass spectrometer (ICP-MS), using NexION 350D instrument. The combined dilution and analytical errors were <10%, except for Ca and K, where only qualitative values were obtained. The calibration curves for each analyte were constructed using standard solutions made fresh for each analytical run.

Hydrostatic compaction experiments.

Grain packs of sieved laumontite with grain sizes 0.425 to 1 mm were deformed hydrostatically under hydrothermal conditions to observe pressure related changes due to chemically induced dehydration reactions. Samples were prepared using granular laumontite poured into preformed jacketing to form samples 26mm in diameter, and 29 mm long. Hastelloy frits were used on both ends of the sample to contain the loose grains and distribute pore fluids evenly across the ends of the sample at pressure. A three-layer jacket procedure was used to isolate the sample from the confining pressure and minimize diffusion of water that could occur at high temperatures and extended time periods. A 0.05 mm thick annealed nickel foil was sandwiched between two 0.5 mm thick PTFE Teflon layers. The jackets were secured to the end caps with two nickel-chromium tie wires. Titanium end caps were used to minimize corrosion during experiments (Figure 1a).

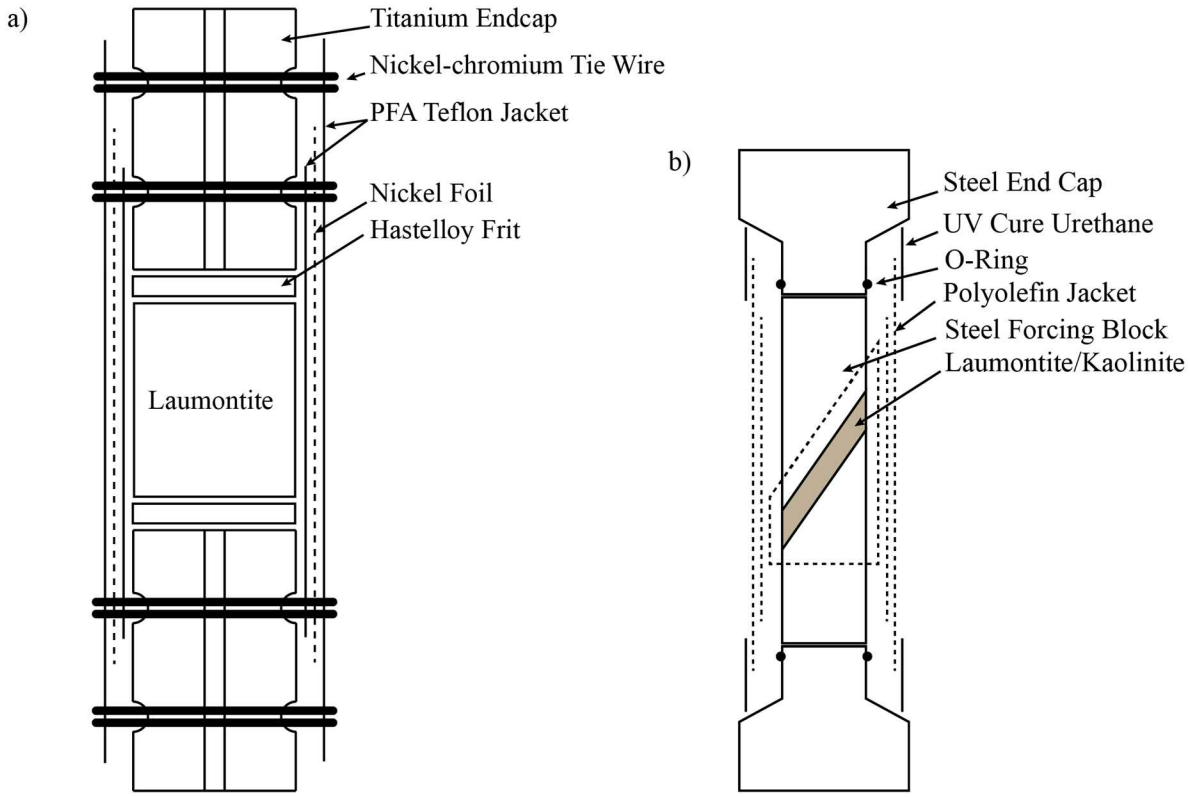

Figure 1. Sample geometry used in a) compaction and b) friction experiments.

Samples were deformed using a Newport Scientific SuperPressure hydrostatic vessel. Samples were initially loaded to 1.7 MPa confining pressure, P_C. Pore fluid was introduced into the sample via an Isco syringe pump from the bottom of the sample to ensure even saturation. Pore fluid pressure, P_P, was increased to 0.7 MPa. P_C was increased to 8.6 MPa and P_P was increased to 6.9 MPa, making sure that effective pressure, P_E=P_C-P_P, never exceeded 1.7 MPa. P_C was increased to 126.9 MPa, and P_P was held at 6.9 MPa to monitor the change in pore fluid volume. P_E was held at 120 MPa for 1 hour, and P_C was reduced to 81.9 MPa while P_P remained at 6.9 MPa. Temperature was increased to 85° C using silicone heater blankets on the outside of the vessel. Once at temperature, the pore fluid Isco pump was valved off, and a HiP screw driven pressure generator was used to maintain a constant pressure value, measuring changes in pore volume at high resolution. The sample was allowed to creep at 75 MPa P_E and 85° C for 1 week. The initial loading overcompacts the sample to prevent creep from mechanical loading the 1-week hold. Any volume changes observed during the elevated temperature step should result from fluid-rock interactions. Experiments were conducted using the same pore fluids as the PARR experiments: DI H_2O, 1M NaCl pH 9, 1M NaCl pH 6, and 1M NaCl pH 3, all fluids equilibrated with atmospheric CO_2 pressures. After experiments, samples were vacuum impregnated with rhodamine dyed low viscosity epoxy and prepared into thin sections. An additional experiment was performed dry without the creep period to determine the porosity after mechanical loading. Thin sections were investigated using a petrographic microscope and scanning electron microscope, SEM. SEM observations and analyses were conducted with a TESCAN Vega3 Scanning Electron Microscope operated at 20.0 kV. Elemental analyses using the TEAM EDS system were also conducted to aid in identifying minerals of interest.

Friction experiments.

Friction experiments were conducted on fine grained laumontite – kaolinite mixtures to understand changes in fault strength to dehydration reactions. Samples were prepared as different percentages by weight: 100% laumontite, 75% laumontite – 25% kaolinite, 50% laumontite – 50% kaolinite, 25% laumontite – 75% kaolinite, and 100% kaolinite. Rigid steel forcing blocks were used to deform the mixture as simulated fault gouge under triaxial compression loading. 12.5 mm diameter steel cylinders with a 35° inclined face were used as forcing blocks; the inclined face of the blocks were machined with fine grooves to prevent slippage at the interface of the gouge. 0.3 – 0.7 g of powders were applied evenly across the face to create a 3-mm thick layer. The ends of the steel blocks were lubricated with a mixture of Vaseline and stearic acid to minimize friction with the endcaps. Samples were jacketed with 3 layers of heat shrink polyolefin tubing. The inner two layers were applied over the steel forcing blocks. The outer layer was sealed the sample to the endcaps over O-rings to form an impermeable seal (Figure 1b). The endcap – sample union was coated with a UV cure urethane for additional protection. In order to establish a steady state sliding condition in these samples

with limited displacement, a P_C reduction load path was employed. Samples were loaded hydrostatically to 30 MPa, and then loaded axially to 75 kN. The axial load, σ_A, was held constant while P_C was lowered to 1.7 MPa. σ_A was lowered, and P_C was returned to 30 MPa. The next stage of loading deformed the sample a constant normal stress, σ_n, while shear stress, τ, was allowed to vary in order to calculate the coefficient of friction, μ, where

$$\tau = (\sigma_A - P_C)\sin\theta\cos\theta, \quad (4)$$

$$\sigma_n = P_C + (\sigma_A - P_C)\sin^2\theta, \quad (5)$$

and

$$\mu = \tau/\sigma_n. \quad (6)$$

θ is the angle of the face of the forcing blocks, 35°. The sample was deformed at a constant axial displacement rate while P_C was continuously adjusted to maintain a constant σ_n. All experiments were performed at 30 MPa σ_n. Axial displacement rates were stepped between 0.01, 0.001, and 0.0001 mm/sec. 100 and 1000 second holds were also employed were the axial displacement was stopped while maintaining a constant normal stress. Samples were displaced at 0.001 mm/sec for 2 mm, displacement velocity was increased to 0.01 mm/sec, decreased to 0.0001 mm/sec, increased to 0.001 mm/sec, and then displacement was held for 100 seconds. The samples were then deformed at 0.001 mm/sec, then 0.0001 mm/sec, 0.01 mm/sec, 0.001 mm/sec, and displacement was held for 1000 seconds. Samples were deformed at 0.001 mm/sec to reestablish loading and then unloaded. Total deformation in the constant σ_n portion of loading was >4 mm.

RESULTS:

Laumontite reaction modelling

The current analysis assumes laumontite dehydration to produce kaolinite, $SiO_{2(aq)}$, Ca^{++}, and H_2O. Thermodynamic evaluation of these mineral assemblage equilibria can be described using the equations 2 and 3 defined earlier. Figure 2 shows the logK of reactions (2) and (3) as a function of temperature considering both $CO_{2(gas)}$ and $CO_{2(aq)}$. The curves are computed along the liquid-vapor saturation pressure of pure H_2O. In this case we assume $CaAl_2Si_4O_{12}$•$3.5H_2O$ ("leonh") or "leonhardite" as the stable laumontite phase even at low temperatures. Notice that the carbonate-absent reaction is favored with decreasing logK as temperature increases.

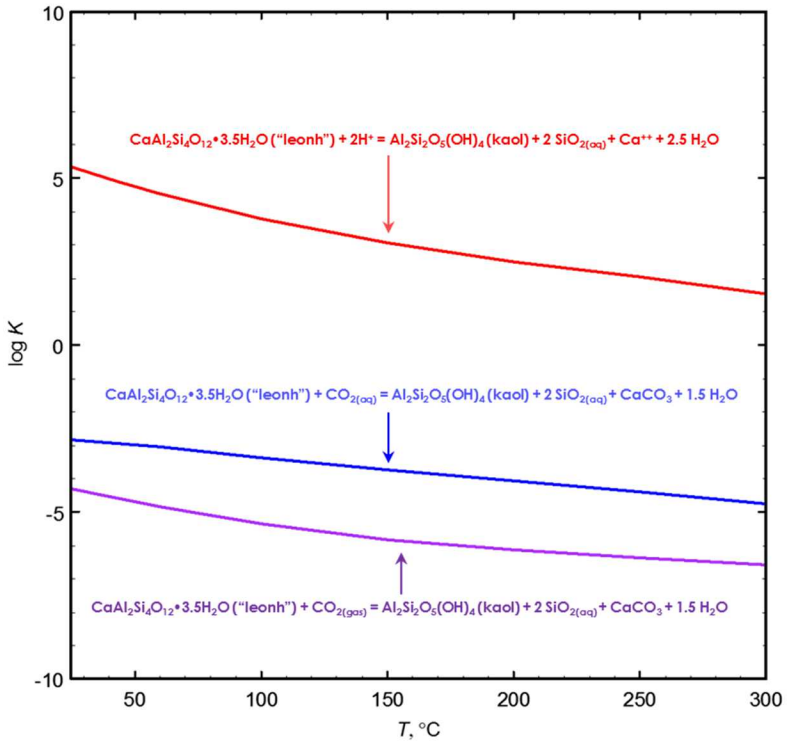

Figure 2. LogK vs. temperatures for reactions (1) and (2) considering $CO_{2(gas)}$ and $CO_{2(aq)}$ computed using the CHNOSZ software and thermodynamic for the laumontite phases from *Neuhoff and Bird* [2001].

Using the required thermodynamic data for the laumontite phases to extrapolate as a function of pressure and temperature, we can analyze dehydration reactions for these phases given by the following reaction:

$$CaAl_2Si_4O_{12}•4.5H_2O\ (lmt) = CaAl_2Si_4O_{12}•3.5H_2O\ (\text{“leonh”}) + H_2O \qquad (4)$$

The mass action law expression for reaction (4) is given by:

$$K = \frac{a_{\text{"leonh"}}\, a_{H2O}}{a_{lmt}} \qquad (5)$$

Assuming unit activity for the end-member solids, Eqn. 5 can be used to relate the equilibrium relative humidity (RH), a_{H2O}, and the standard Gibbs energy of the reaction, K.

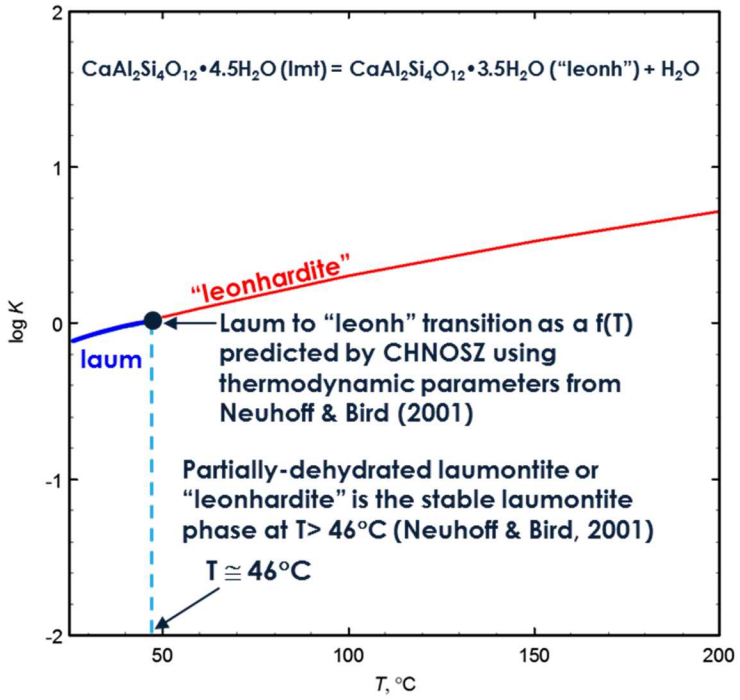

Figure 3. LogK profile as a function of temperature for reaction (3) using CHNOSZ and thermodynamic given in *Neuhoff and Bird* [2001] – see text.

Figure 3 shows a plot of logK vs. temperature for reaction (4) where K is defined by Eqn. (5). The transition from laumontite to "leonhardite" at a temperature of ~46°C is constrained by the analysis of heat capacity data by Neuhoff and Bird [2001]. Although the precise temperature at which this transition occurs is still debated [*Fridriksson et al.*, 2003], the thermodynamic analysis of *Neuhoff and Bird* [2001] advances data parameters consistent with laumontite dehydration to "leonhardite" at ambient conditions. Further, these authors argue that the stable laumontite phase to be considered in the analysis of zeolite stability relations at elevated pressures and temperatures is "leonhardite". It should be noted that the change in volume in these reactions is also important to fluid generation and hence pore pressures but also to the stability of other hydrous silicate phases.

This thermodynamic analysis can be extended to the generation of activity phase diagrams to represent the stability relations of the mineral assemblage. Figure 4 depicts an activity phase diagram based on the aCa^{++}/a^2H^+ ratio as a function of temperature constructed using CHNOSZ (with mosaic option). It captures transition of laumontite to "leonhardite" and the stability relations with respect to kaolinite. The diagram assumes fixed activities of Al^{+++} and $SiO_{2(aq)}$ as well as pH allowing for mapping of phase stabilities for a wide range of compositions as a function of temperature. Figure 4 shows that a Ca-deficient solution favors the formation of kaolinite with increasing temperature. The amount of carbonate in this case is very small

therefore calcite is not part of the assemblage. Changing the assumed activities of Al^{+++} and $SiO_{2(aq)}$ will influence the size of the stability fields which is useful in the evaluation aqueous component sensitivities to the occurrence of these phases.

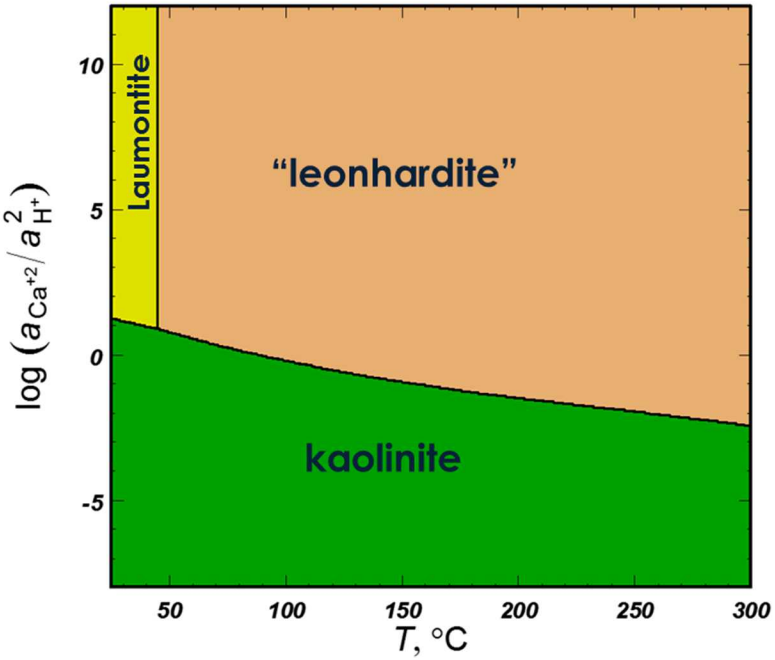

Figure 4. Activity phase diagram of aCa^{++}/a^2H^+ ratio as a function of temperature showing the predominance fields of the mineral assemblage of interest in the absence of CO_2. The diagram is constrained to a neutral pH and activities of Al^{+++} and $SiO_{2(aq)}$ of 10^{-5}.

Figure 5 shows a similar activity phase diagram but with the presence of carbonate allows the formation of calcite. Notice the effect on the phase topology with the added phase. The invariant point between "leonhardite", kaolinite, and calcite located ~100°C but changes in the diagram constrains (i.e., species activities) will shift it to other temperatures. Such equilibria mapping is often useful in constraining fluid composition for a given mineral assemblage and the design of experiments targeting specific reaction products. In this study, the formation of kaolinite from laumontite appears to be feasible under moderate temperatures. This analysis also show that carbonate-free conditions favor kaolinite formation. However, dissolution and precipitation kinetics can play a key role in determining the extent of this reaction which at low temperatures are known to be slow.

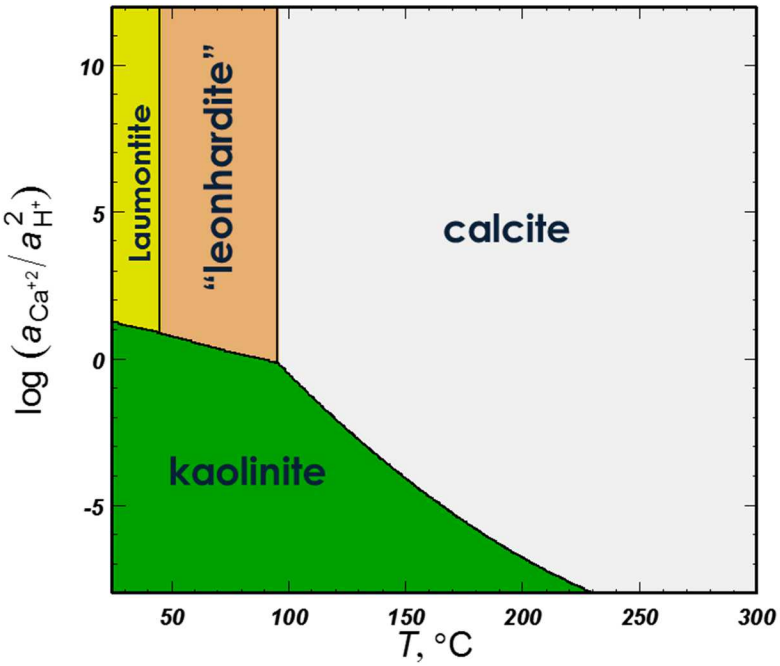

Figure 5. Activity phase diagram of aCa^{++}/a^2H^+ ratio as a function of temperature showing the predominance fields of the mineral assemblage of interest in the presence of CO_2. The diagram is constrained to a neutral pH and activities of Al^{+++} and $SiO_{2(aq)}$ of 10^{-5}. The activity of CO_3^{--} constrained to 10^{-7}.

Characterization of materials

Two forms of "laumontite" mineral mixtures were received: fine grained powders, and coarse grained granular form. Both mixtures contained only minor amount of laumontite, with the main phase being albite (Figure 6, and Table 1).

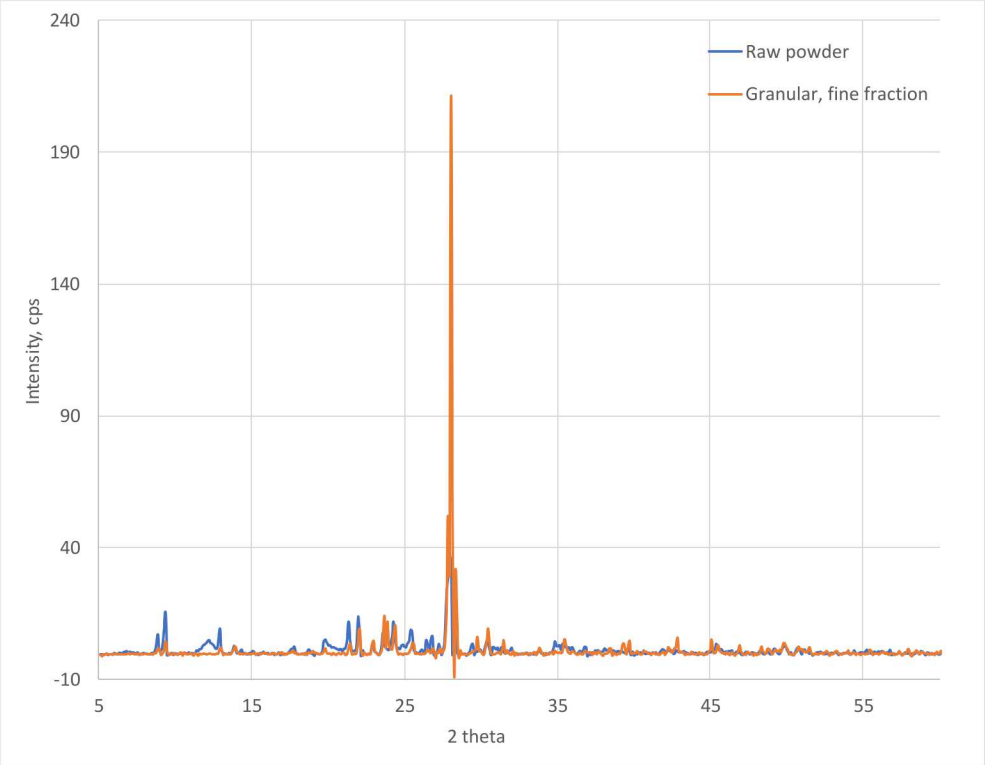

Figure 6. X-ray diffraction patterns for the received laumontite materials. Both powder and granular materials are predominantly made of albite (see Table 1 for composition).

Purification procedure and characterization of purified phase

Laumontite powder received from the source contained albite, muscovite, laumontite, and kaolinite (Table 1). The predominant phase in this mixture was albite. We performed density separation, using sodium polytungstate solution (NaPT) to enrich laumontite phase in the sample. The XRD patterns before and after the purification procedure are shown in Figure 7. The purification procedure resulted in a decrease in the albite signal, however, heavy liquid separation was not able to eliminate albite from the mineral mixture. Most notably, the purification procedure led to a significant increase in the kaolinite fraction (Figure 7). Since purification procedure did not significantly enrich laumontite fraction in the mineral mixture, we used the received mineral powder "as is" for the alteration experiments.

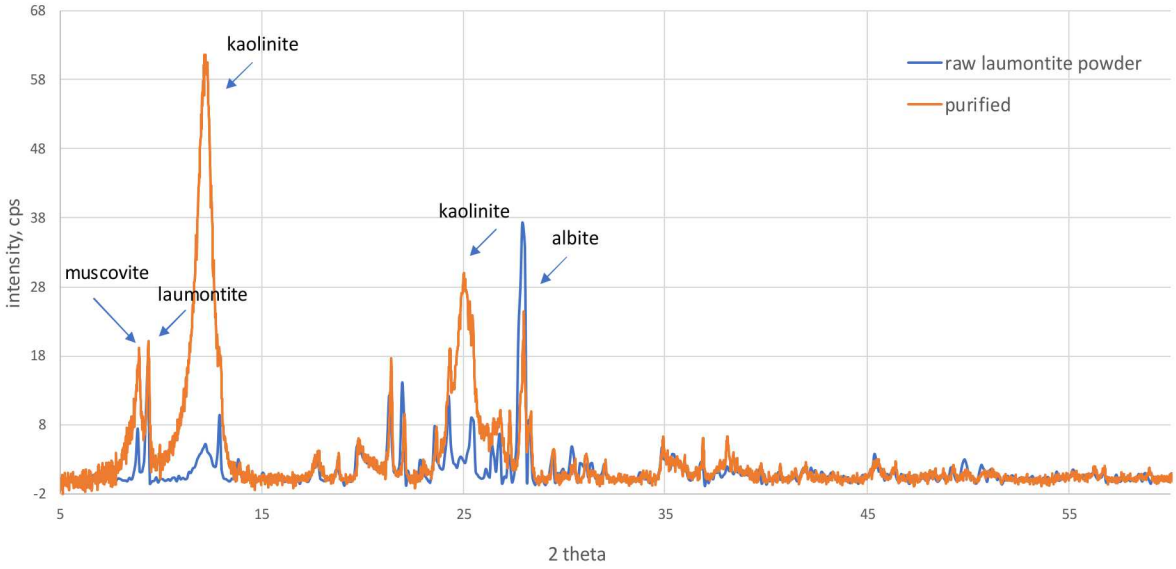

Figure 7. X-ray diffraction patterns for the laumontite powder before and after density separation, using sodium polytungstate (NaPT).

Alteration experiments

A total of 7 alteration experiments were run, each lasting 8 weeks. At the completion of the experiments, solid and liquid phases were separated and analyzed. The solid and aqueous phases collected from the reactors indicate slight mineralogical alteration, which was dependent on the aqueous composition of the reactors. The semi-quantitative results for the solid-phase composition are shown in Figure 3 and Table 1. In de-ionized water, due to partial dissolution of the parent mineral phases, new smectite-type phase was forming (Figure 8). In the other three powder reactors, we observed the formation of a new fine-grained phase (vermiculite), which was not detected in the un-reacted mineral powder.

The extent of dissolution was similar in all reactors, with slightly higher extent of dissolution in the powder reactors at pH 3 and in the presence of CO_2, and in the granular reactor with CO_2. The presence of Ca in the solution is indicative of laumontite dissolution. Calcium concentrations were higher in the powder reactors, compared to the granular reactors, consistent with a higher abundance of laumontite in the powder mixture (Table 1). Similarly, in the granular reactors a minor amount of vermiculite has formed following the alteration treatment (data not shown). No kaolinite was observed in the granular reactors following the alteration experiment.

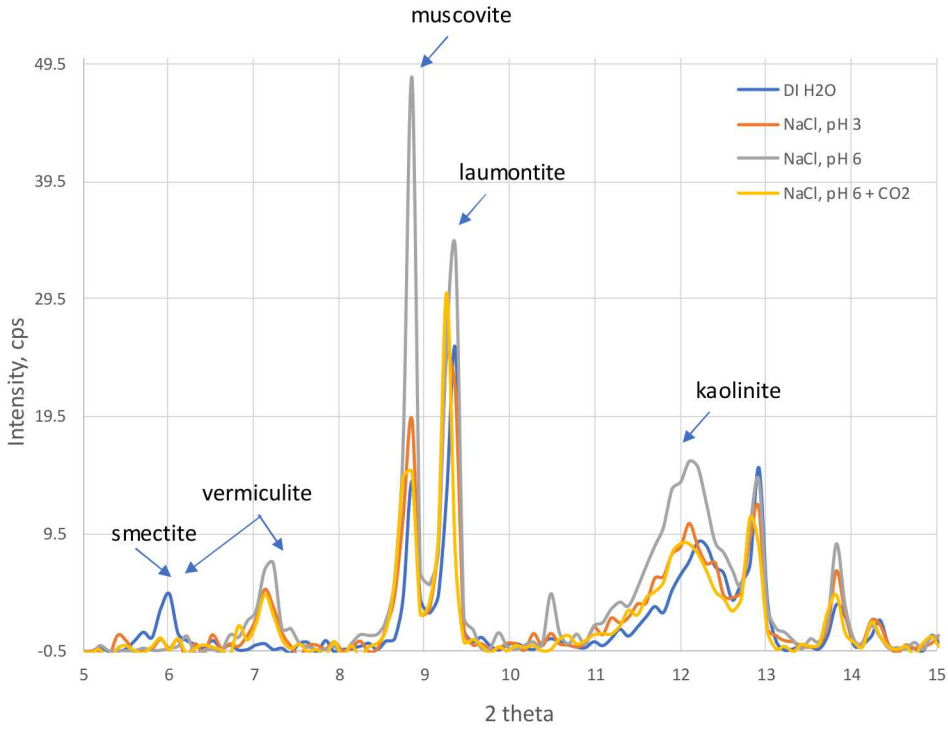

Figure 8. X-ray diffraction patterns for the laumontite powder before and after alteration experiments.

Table 1. Semi-quantitative mineralogical composition of laumontite mineral mixtures before and after alteration experiments.

Reactor	**Laumontite, $CaAl_2Si_4O_{12}•4(H_2O)$ wt.%**	**Albite, $NaAlSi_3O_8$ wt. %**	**Muscovite, $KAl_2(Si_3Al)O_{10}(OH,F)_2$ wt.%**	**Kaolinite, $Al_2Si_2O_5(OH)_4$ wt.%**
Powder reactors				
Laumontite powder	8.0	69.0	17.7	5.3
1. Powdered laumontite in de-ionized H_2O	10.2	59.4	21.9	8.5
2. Powdered laumontite in 1M NaCl at pH 3	8.4	58.9	27.3	5.4
3. Powdered laumontite in 1M NaCl at pH 6	5.5	56.3	32.6	5.6
4.Powdered laumontite in 1M NaCl, initially at pH 6 with CO_2	9.1	64.8	18.9	7.2
Granular reactors				
Unreacted	3.1	93.5	2.8	0.5

5. Granular (< 0.425 mm) laumontite in 1M NaCl at pH 3	0.9	93.7	5.4	0
6. Granular (< 0.425 mm) laumontite in 1M NaCl at pH 6	0.4	94.2	5.4	0
7. Granular (< 0.425 mm) laumontite in 1M NaCl, initially at pH 6 with CO_2	1.1	97.3	1.6	0

Table 2. Aqueous composition of the reactors after the alteration experiment. Sodium and chloride are not reported.

Sample Id	Ca [a)] (ppb)	Mg (ppb)	K [a)] (ppb)	Si (ppb)	Fe (ppb)	Al (ppb)	Sr (ppb)
1. Powdered laumontite in de-ionized H_2O	921	147	956	35933	8	73	20
2. Powdered laumontite in 1M NaCl at pH 3	8546	2644	3163	34521	0	2	1330
3. Powdered laumontite in 1M NaCl at pH 6	8568	2479	3429	22455	0	0	1348
4. Powdered laumontite in 1M NaCl, initially at pH 6 with CO_2	9244	2607	3627	26306	0	0	1428
5. Granular (< 0.425 mm) laumontite in 1M NaCl at pH 3	4306	774	1064	22369	54	787	862
6. Granular (< 0.425 mm) laumontite in 1M NaCl at pH 6	4073	731	1034	13115	0	9	975
7. Granular (< 0.425 mm) laumontite in 1M NaCl, initially at pH 6 with CO_2	4970	887	1134	33404	1312	1524	1126

Note:
[a)] Due to mass-interferences, reported concentrations of Ca and K are qualitative.

Hydrostatic compaction experiments.

A total of four compaction experiments were performed on granular laumontite samples. Samples were precompacted in the presence of different fluids before increasing temperature to induce chemical reactions. Different fluid chemistries did not affect compaction, as total strain and strain during the hold are similar for all samples. For NaCl pH 3, there was a leak in the

syringe pump that has been corrected for, leading to a higher estimate of strain during the 1-hour hold period. After the samples had reached temperature and the creep period had begun, the responses for DI H_2O, NaCl pH 9, and NaCl pH 6 are very similar (Figure 9). Initially, pore pressure increases, likely a result of the system equilibrating at elevated temperatures. Pressure equilibrates and the samples are stable. At the end of the experiment, pressure increases in the DI H_2O sample, indicating a decrease in porosity. The NaCl pH 6 and 9 brines demonstrate a decrease in pore pressure at the end of the experiment, indicating either the sample dilated, or fluids were consumed by chemical reactions or adsorption into the crystal lattice. In the NaCl pH 3 solution, pore pressure dropped significantly during the initial creep phase. This could indicate a pressure leak, but no signs of leaks were observed and pressure equilibrated over time (Figure 9). Absent of leaks in the system, the drop in pore pressure resulted from interactions of the acidic fluid with laumontite powders. Water present in the brine could have adsorbed into the crystal lattice, lowering pore pressure. Dehydration of laumontite into kaolinite could have also created additional pore spaces, decreasing pore pressure.

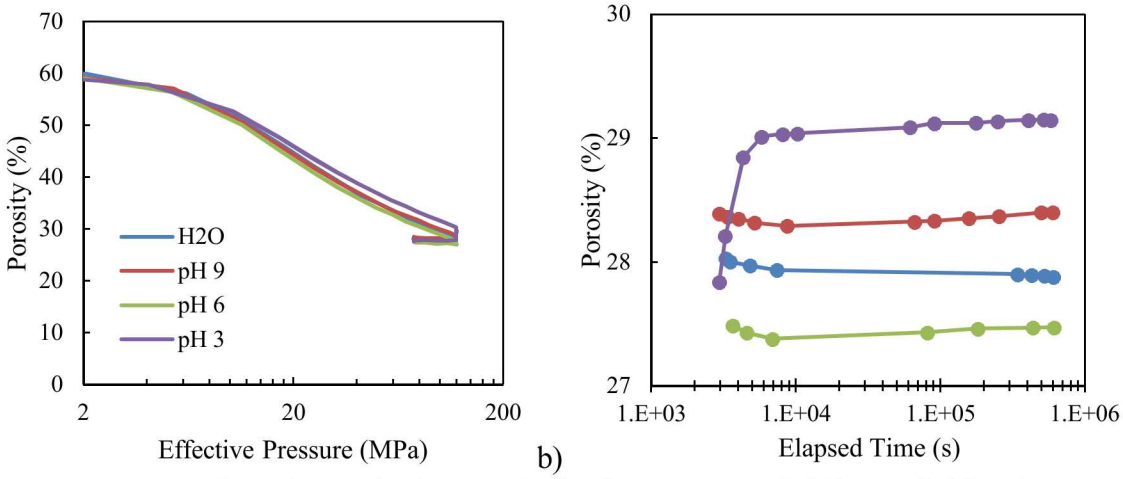

Figure 9. Compaction of granular laumontite in the presence of different fluids. a) Over compaction curve from room temperature portion of experiments. b) 1 week hold at 85° C.

Table 3. Results of hydrostatic compaction experiments.

Sample ID	Fluid	Porosity from Pore Volume Calculations	Porosity Change During Loading	Porosity Change During Creep	Measured Porosity
2	H2O	26.96	31.96	0.16	21.9
3	1M NaCl pH 9	27.7	31.6	0	26.1
4	1M NaCl pH 6	26.45	31.97	0.06	29.7
5	1M NaCl pH 3	32.37	31.35	-1.5	34.3

Microstructures of deformed samples.

Microstructural investigation show that samples deformed due to compaction, grain crushing, and comminution for all fluid types. Undeformed grains are primarily albite (A) with varying degrees of alteration and intragranular microfracturing, but largely intact grains (Figure 10, 11a). Deformed samples have low porosities due to compaction and partial filling of pore spaces and microfractures with comminuted grain fragments (Figure 10, 11). Microfracturing of grains is preferred at point contacts between grains and in grains that are preferentially oriented for failure along cleavage planes. BSE and SE images from Sample 3 pH9 show microfractured albite (A) and kaolinite (K), heavily fractured laumontite (L), and pore fill in between consisting of a variety of grain fragments (Figure 11c, d). Grain fragments are roughly aligned with larger grain boundaries, and do not show evidence of alteration or post-deformation mineralization. This suggest that fine grained kaolinite occurring as fracture fill resulted from mechanical deformation, and did not form in situ. No alteration products are visible on deformed laumontite grains (Figure 11d, e).

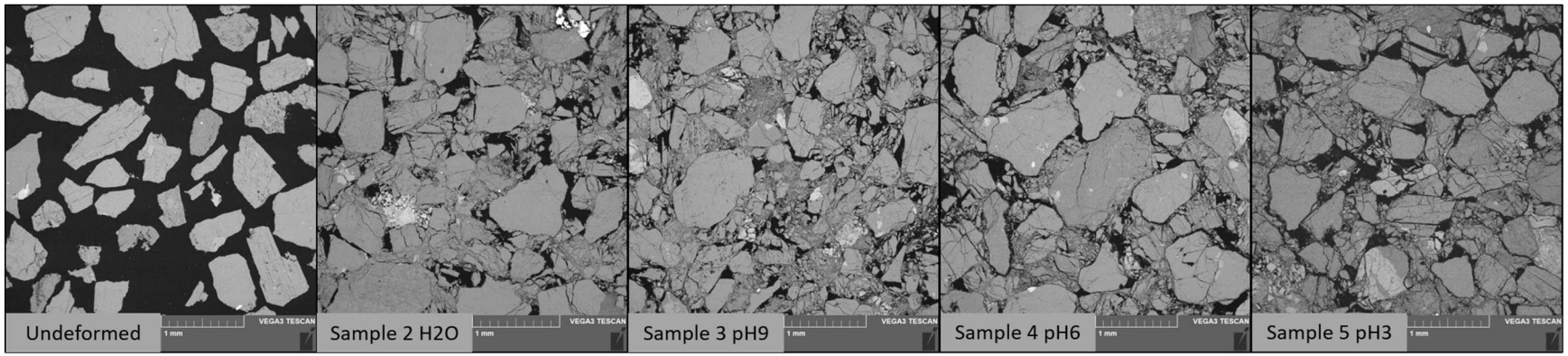

Figure 10. BSE images of undeformed and all deformed samples. Porosity in black is greatest in the undeformed sample and decreases due to compaction, grain crushing, and comminution in deformed samples. Grains (gray) consist of mostly albite with some laumontite, biotite, and kaolinite, and rare quartz, potassium feldspar, siderite, and other unidentified opaque minerals and lithic fragments.

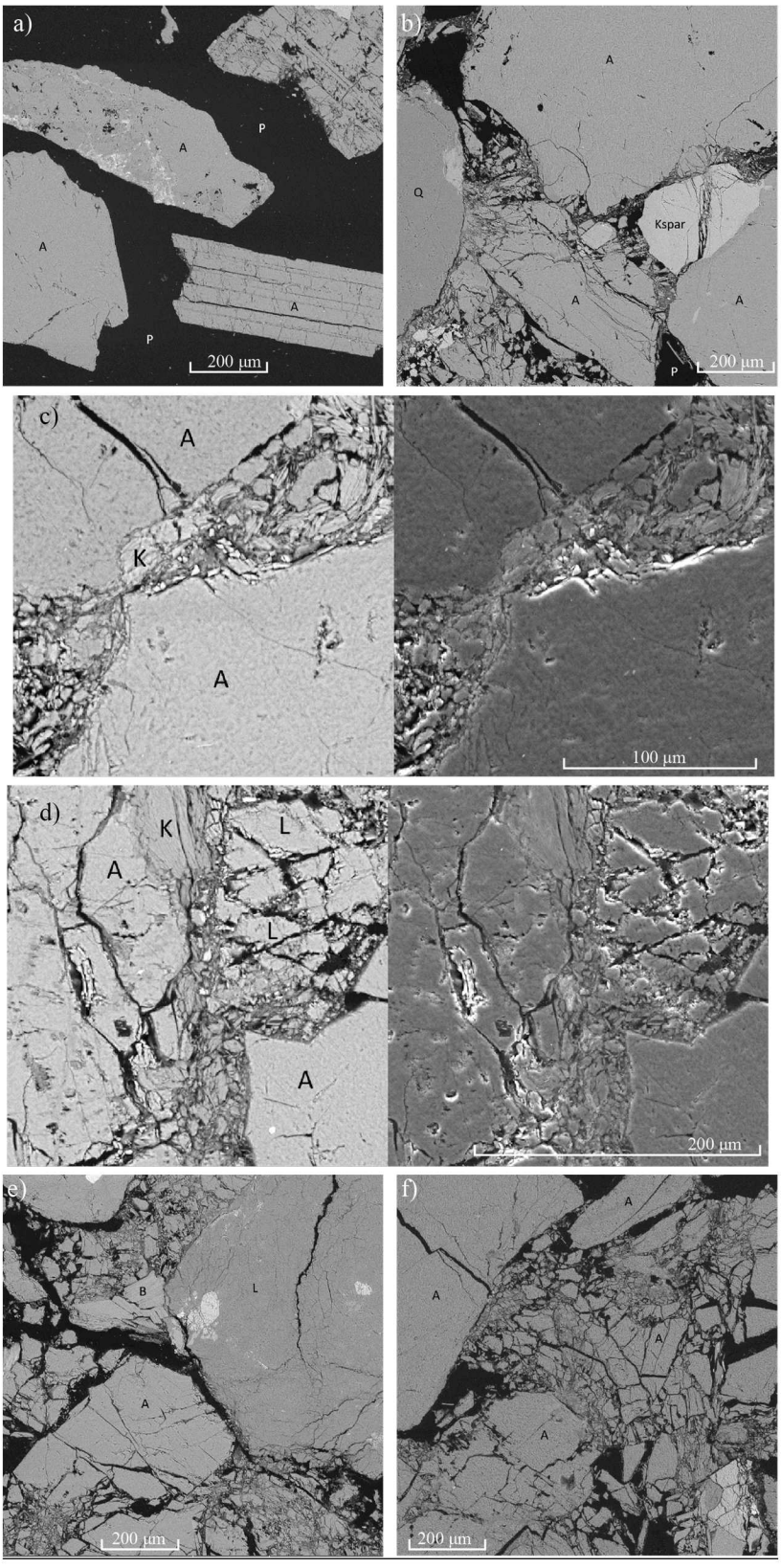
a)
P
A
A
A
P
200 µm
b)
A
Q
Kspar
A
A
P
200 µm
c)
A
K
A
100 µm
d)
K
L
A
L
A
200 µm
e)
B
L
A
200 µm
f)
A
A
A
A
200 µm

Figure 11. BSE images showing deformation of granular laumontite. a) undeformed grains. b) Sample 2, DI H_2O. c,d) Sample 3, 1M NaCl pH 9. e) Sample 4, 1M NaCl pH 6. f) 1 M NaCl pH 3.

Friction experiments.

A total of 5 friction experiments were conducted on different mixtures of laumontite – kaolinite powders. Composition varied from 100% laumontite to 100% kaolinite in 25% increments. Samples were deformed under a P_C reduction load path to form slip surfaces and reach steady state slip with limited displacement. This step was followed by constant axial displacement at a constant normal stress value of 30 MPa. All experiments were conducted to 4+ mm axial displacement under constant normal stress without rupturing a jacket (Figure 12). Axial displacement rates were stepped from 0.001 mm/sec to 0.01 mm/sec to 0.0001 mm/sec to 0.001 mm/sec to 0.0001 mm/sec to 0.01 mm/sec to 0.001 mm/sec. 100 and 1000 second holds were performed during 0.001 mm/sec displacement rates. Values of the coefficient are similar for different compositions, but the stability of the different mixtures vary greatly. The coefficient of friction for laumontite and kaolinite is 0.71 for pure compositions, but laumontite exhibits stick-slip behavior while kaolinites slides smoothly. The behavior of the mixes displays intermediate behavior to the two end members (Figure 13). The 75% kaolinite – 25% laumontite mixture has a 0.71 coefficient of friction and displays a slightly higher tendency for stick-slip behavior than the pure kaolinite mixture. The 50% laumontite – 50% kaolinite mixtures and 75% laumontite – 25% kaolinite mixtures have a lower coefficient of frictions at 0.66. The mixtures exhibit stick-slip behavior, and the tendency for slip events increase with increasing laumontite content (Figure 13).

Figure 12. Sample after deformation.

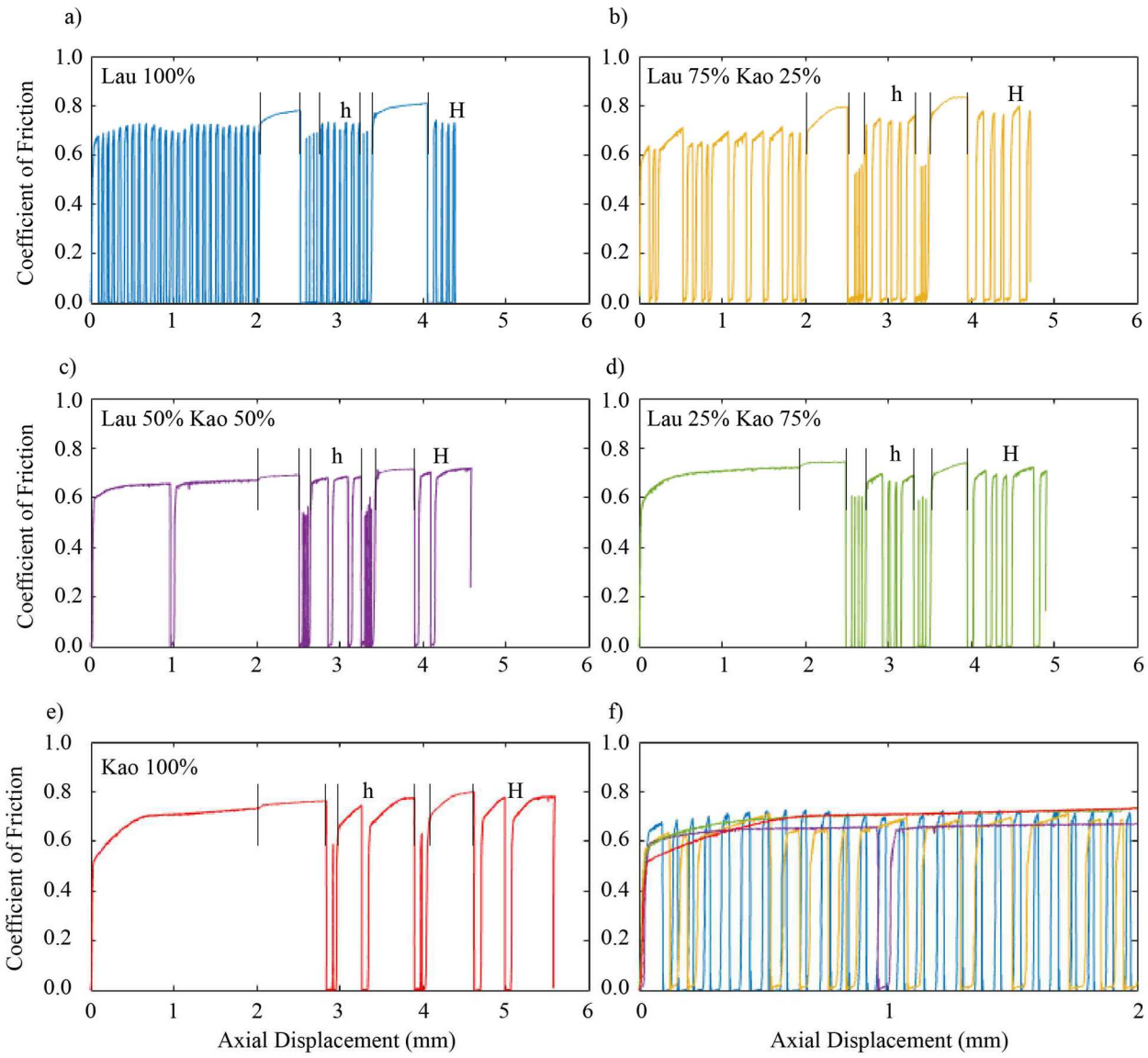

Figure 13. Result from friction experiments on laumontite-kaolinite mixes. Changes in axial displacement are marked by vertical black lines. "h" denotes 100 second hold, "H" denotes 1000 second hold. a) 100% laumontite powder. b) 75% laumontite – 25% kaolinite mix. c) 50% laumontite – 50% kaolinite mix. d) 25% laumontite – 75% kaolinite mix. e) 100% kaolinite mix. f) Comparison of different mixes at 0.001 mm/sec displacement rates.

DISCUSSION:

The experiments in this study were conducted on different grain sized fractions of laumontite from a commercial source with sufficient quantities available for experimental studies. The actual percentage of laumontite in the purchased samples are low: ~8% for

pharmaceutical grade powder and ~3% for the granular samples. Attempts to purify the samples were unsuccessful. Heavy liquid separation reacted with the fine-grained samples to increase kaolinite contents, and neither separation or settling techniques proved effective with the granular samples. The mineralogy of the samples was albite, laumontite, muscovite, and kaolinite. While not pure laumontite, the mix of minerals reflect the mineralogy of fault and fracture systems in crystalline basement formations, so responses of these samples are indicative of the behavior the whole fracture system to new fluid chemistries.

Chemical reaction experiments and compaction experiments exposed samples to different fluid chemistries intended to induce dehydration reactions in laumontite. Themodynamic modelling of laumontite, "leonhardite", and kaolinite systems indicate that the conditions of our experiments should trigger dehydration of laumontite to kaolinite. Long term PARR experiments did not document this reaction with any of the fluids. There was evidence for laumontite dissolution, but no kaolinite precipitated (Table 2). Fine powders exposed to 1M NaCl solutions precipitated vermiculite, and powders exposed to DI H_2O precipitated smectite (Figure 8). The formation of the fine-grained alteration products is expected to alter the slip behavior of faults. Compaction experiments were conducted on a shorter time frame than PARR experiments, but increases in surface area from fractured grains should increase reactivity of grains. Significant mineralogical differences were not apparent between samples deformed with different fluids. All samples compacted by extensive grain crushing and mica/clay plasticity, but dissolution-precipitation structures were not observed (Figure 10, 11).

The porosity decrease in granular laumontite after exposure to different fluids were similar. Samples compacted a similar amount during the loading, and volume changes during the 1 week hold time are small. For the samples exposed to DI H_2O, 1M NaCl pH 9, and 1M NaCl pH 6, the fluid-rock interactions would not affect the mechanical behavior of the sample. For in situ faults in crystalline basement formations, the results from this study suggest that neutral to basic fluids would not affect seismicity beyond pore pressure effects from pumping and diffusion. The sample exposed to 1M NaCl pH3 brine observed a decrease in pore pressure, either due to adsorption into mineral grain structures or the creation of porosity from chemical reactions. PARR experiments did not observe significant laumontite dissolution, so it is unlikely that the observed pressure behavior is due to volume decreases created by the dehydration reaction of laumontite to kaolinite. Likely, the decrease in pore pressure is related to adsorption of water into grain structures and alterations in clay structures. In nature, this would indicate that acidic fluids introduced into crystalline basement fault networks would reduce the risk of induced seismicity. Fluid-rock interactions would counterbalance increases in pore pressure due to injection, delaying seismicity until the fault mineralogy equilibrates with the newly introduced fluids. This would suggest that observations of delayed seismicity from injection could be due to the effect of acidic fracking fluid and produced water creating a new chemical equilibrium in basement faults. Reactions would help buffer pore pressure increases, and after a new

equilibrium had been established, pore pressure would be determined by pumping and hydraulic diffusivity.

The coefficient of friction is similar for the fine grained laumontite powder and pure kaolinite, suggesting that the completed dehydration reactions would not alter fault strength. Both samples have a high coefficient of friction, 0.71, that would lead to high shear stresses along faults. Mixture of fine grained laumontite and kaolinite have lower coefficients of friction, 0.66, than either end member sample. This reduction would lower fault strength and could trigger seismicity. Observations of faults and fractures in nature indicate that stresses along active faults are at frictional limits, and hydraulically connected faults are most likely active [*Zoback*, 2010]. Under the critically stressed fault theory, fault networks in basement formations would be near frictional limits. Pore pressure increases as small as 0.001 – 0.1 MPa were sufficient to trigger slip in the KTB experiment [*Shapiro et al.*, 2006], so it is likely that the small change in coefficient of friction (~0.05) could affect the potential for induced seismicity. As the dehydration reaction initiates in laumontite fault and fracture fill, the coefficient of friction would decrease. The experiments indicate the coefficient of friction would be constant as the composition changes until kaolinite content reaches 75%, when the coefficient of friction is the same as pure kaolinite.

The change in slip behavior from laumontite to kaolinite is a novel observation. Fine grained laumontite powders demonstrate episodic slip, or stick-slip, behavior with deformation. This slip behavior occurs at displacement rates of 0.001 mm/sec and 0.0001 mm/sec, and not at the fast displacement rate of 0.01 mm/sec. Slip occurred at repeatable distances, and this distance did not change with displacement. With increasing kaolinite content, the tendency for stick slip decreased. The 25% and 50% kaolinite mixtures show stick-slip behavior for the slow and medium velocities, but the 75% kaolinite mixture shows stick-slip behavior only at the slow velocities and after the displacement holds. Pure kaolinite displays slip only at slow velocities, consistent with previous experimental observations of partial velocity weakening behavior [*Ikari et al.*, 2011]. Stick-slip behavior observed in experiments is similar to stick-slip behavior observed on natural faults during earthquakes. This study indicates that the laumontite fault and fracture fills would be prone to earthquake as opposed to aseismic sliding or creep. The potential for earthquakes would be reduced as dehydration reaction increase kaolinite content, but kaolinite still has the potential for unstable slip.

The experiments in this study portray conflicting results in the context of induced seismicity in basement faults. PARR and compaction experiments demonstrate that the kinetics of the laumontite dehydration reaction are slow on laboratory time scales. We did not observe significant conversion of laumontite to kaolinite over a 8-week period, but this does not preclude that the reaction would not occur in the field. Disposal wells are active over a timespan of years, so the reaction could be significant over the time span of the well. Elevated temperature that could be present along deeper portions of basement faults could also increase the kinetics of the

reaction. Lower fluid to solid ratios in nature could result in higher precipitation rates. The results do suggest that the rate of dehydration reactions would not exceed the hydraulic diffusivity of fault and fracture networks, so pore pressure changes from dehydration would be negligible. The compaction experiment at pH 3 observed a decrease in pore pressure, which would inhibit fault reactivation. Previous experiments on laumontite cemented sandstones exposed to CO_2 enriched brines observed the reaction of laumontite to kaolinite in 1-week experiments, suggesting that CO_2 sequestration projects in basal sedimentary formations could trigger unexpected seismicity [*Luquot et a., 2012*]. Friction experiments on analog fault gouge compositions suggest that converting laumontite to kaolinite would affect fault behavior. At low kaolinite compositions, coefficient of friction is reduced, which could be significant on critically stressed faults. When kaolinite is a majority of the fault gouge, the coefficient increases, increasing fault strength. Slip behavior changes as well. The tendency for unstable slip still exists, but less than the original laumontite fault gouge. Injecting acidic fluids into basement fault systems would cause a temporary drop in pore pressure, stabilizing the fault. As laumontite dehydrates to kaolinite, the fault would weaken, which could trigger seismicity. Neutral to high pH fluids would avoid time dependent changes in fault strength, and seismicity would be determined by pumping.

ANTICIPATED OUTCOMES AND IMPACTS:

This project focused on the induced seismicity problem in the midcontinent US through a focused investigation into the behavior of analog fault and fracture fill. Induced seismicity is caused by high volume injection wells disposing of used fracking fluids and produced waters from unconventional petroleum resources. The magnitudes of induced events are increasing, and these events are occurring in locations that have lacked historical seismicity and are vulnerable to seismic damage. Magnitude 5+ events are occurring near Cushing, OK, a critical pipeline and storage hub for crude oil. It is also in the national interest to continue producing oil and gas from unconventional reservoirs. These resources have changed the domestic energy landscape, creating opportunities in power generation and several manufacturing industries. Natural gas power plants are ideal to balance renewable sources of electricity, helping to mitigate climate change. Solutions to, or a greater understanding of, the induced seismicity problem could have far reaching impacts.

To investigate the induced seismicity problem, we assembled a multi-disciplinary team with experts in thermodynamics, experimental geochemistry, petrology, and geomechanics. We addressed the issue by investigating coupled chemical-mechanical effects of different fluids on the behavior analog fault gouge material. We took a multi-prong approach: modeling chemical reactions, detailed geochemical experiments, compaction experiments, and fault simulation experiments. We chose to investigate the behavior of laumontite, a commonly observed mineral in fault and fracture networks in crystalline rocks. Our background research and chemical

modeling suggested that laumontite would be unstable in the fluid chemistries being injected in high volume disposal wells. We did not observe the expected reactions in our geochemical and geomechanical experiments. Our observations showed that fluid-rock interactions in low pH brines could act to reduce pore pressure initially, but changes in fault strength would exacerbate slip. The lack of observable reactions in our experiments would suggest that speed of laumontite to kaolinite reactions would be slower than the hydraulic diffusivity of the fault, so dehydration reactions would not create a surge in pore pressure. Any volume change associated with the creation of kaolinite would act to reduce pore pressure, albeit slowly. Our friction experiments demonstrated a continuum behavior between end members of laumontite and kaolinite representing different stage of completion for dehydration reactions. The tendency for unstable slip reduced with increasing kaolinite content, but unstable slip remained a possibility for pure kaolinite. Decreases in the coefficient of friction was observed for mixtures with partial kaolinite contents, but not for mixtures that were majority kaolinite. The decrease was minor, but the reduction in fault could be sufficient to trigger seismicity in critically stressed faults. This suggests that predictions of fault reactivation potential could overestimate fault strength as dehydration reactions initiate. The results of this study suggest the best way to prevent induced seismicity would be to inject acidified fluids and to control injection pore pressures.

This project established and strengthened working relationships between team members, creating a multi-disciplinary team well suited to address chemo-mechanical problems in the future. The research conducted here highlights the complicated nature of fluid-rock interactions, as the interplay between processes can create potential causes and solutions to a given problem. We were able to identify behaviors that could both induce and prevent seismicity over different time periods. This project also increased the base of knowledge inside Sandia for fault related problems. Sandia has strong expertise in geochemistry and geomechanics, but recent research has not focused on fault behavior. We utilized techniques to perform complicated friction experiments for this project, and we would be able to extend these capabilities to more realistic simulations of fault behavior for future projects. This approach, focusing on crystalline basement fault and fracture networks, could be beneficially applied for future projects on deep borehole repository concepts and enhanced geothermal systems. The behavior of laumontite is sensitive to CO_2, so future studies on laumontite could potentially impact carbon sequestration projects.

We applied for a full LDRD based on this concept, but at the time we did not have sufficient data to move forward. We will apply again in the future. Chemo-mechanical effects on friction and fault strength could be significant, but remain unexplored. Previous work has demonstrated that thermal dehydration reactions create complicated behaviors between pore pressure changes, induced microfracture networks, and reaction kinetics. Very few studies have investigated chemical reactions during frictional sliding, despite the importance of this behavior in nature. We will continue to apply for future proposals utilizing the framework established by

this study. The results from this study will be submitted for publication in a peer-reviewed journal.

CONCLUSION:

Induced seismicity in the US is an increasing problem with immediate and potentially far reaching impacts. The majority of events occur along preexisting faults in the underlying crystalline basement. In this study, we investigated the effect of fluid pH on laumontite, a zeolite commonly observed in fault and fracture networks in crystalline formations. Previous research had demonstrated that laumontite is unstable at low pH or at high CO_2 activity, both of which characterize fracking fluids and produced waters being injected into formations overlying the basement. In the presence of these fluids, laumontite dehydrates to kaolinite, creating changes that could impact fault stability. We modelled the thermodynamics of this reaction and conducted experiments to investigate reaction kinetics and mechanical response. We also investigated the frictional behavior of simulated fault gouges representing different stages of completion for the reaction. In geochemical experiments conducted at 90° C for eight weeks on different sized laumontite powders in different fluids, we did not observe significant alteration of the material, with only minor amounts of fine-grained clay mineral formation. In compaction experiments at 85° C for 1 week, we did not observe significant differences in compaction behavior when different fluid types were used. Microstructural investigation of deformed samples did not identify reaction products. Experiments conducted in the presence of 1M NaCl pH 3 observed pore pressure decreases after heating. This could be caused by adsorption of fluids into the cage structure of laumontite, or by altering the structures of clay minerals present in the starting material. The observed response suggests that acidic fluids would be the least likely to induce seismicity, initially. Friction experiments show that laumontite and kaolinite have similar coefficients of friction, but mixtures with partial kaolinite compositions have reduced coefficient of friction. This reduction could be significant on critically stress faults. This indicates that initial dehydration of laumontite into kaolinite would reduce fault strength and potentially induce seismicity, but as the reaction neared completion the fault strength would increase to the original value. The tendency for stick-slip behavior decreases with increasing kaolinite content, but pure kaolinite still exhibits unstable slip.

ACKNOWLEDGEMENTS:

The authors would like to thank Mathew Ingraham, Perry Barrow, and Mike Hileman for their assistance in performing laboratory tests. Adam Forris was instrumental in the design and manufacturing of the steel forcing blocks used in friction experiments. We would also like to thank Austen Tigges for his efforts in sample preparation of the powders. We would like to acknowledge early discussions with Tom Dewers for this project, as well as Fred Chester's recommendation of a P_C reduction load path. We would like to thank Wagner Petrographic for

excellent service in making thin sections, and Mark Troinoff at Zeo-Tech for making sand sized laumontite in addition to the normal fine grained laumontite powders.

This paper describes objective technical results and analysis. Any subjective views or opinions that might be expressed in the paper do not necessarily represent the views of the U.S. Department of Energy or the United States Government.

Built on
LDRD
Laboratory Directed Research and Development

REFERENCES:

Barbot, E., N. S. Vidic, K. B. Gregory, and R. D. Vidic (2013), Spatial and temporal correlation of water quality parameters of produced waters from Devonian-age shale following hydraulic fracturing, *Environmental science & technology*, *47*(6), 2562-2569.

Bernaudin, M., and F. Gueydan (2018), Episodic tremor and slip explained by fluid□enhanced microfracturing and sealing, *Geophysical Research Letters*, *45*(8), 3471-3480.

Blanc, P., A. Lassin, P. Piantone, M. Azaroual, N. Jacquemet, A. Fabbri, and A. Gaucher (2012), Thermoddem: A geochemical database focused on low temperature water/rock interactions and waste materials, *Applied Geochemistry*, *27*, 2107-2116.

Blanpied, M., C. Marone, D. Lockner, J. Byerlee, and D. King (1998), Quantitative measure of the variation in fault rheology due to fluid□rock interactions, *Journal of Geophysical Research: Solid Earth*, *103*(B5), 9691-9712.

Brantut, N., J. Sulem, and A. Schubnel (2011), Effect of dehydration reactions on earthquake nucleation: Stable sliding, slow transients, and unstable slip, *Journal of Geophysical Research: Solid Earth*, *116*(B5).

Bucher, K., and I. Stober (2010), Fluids in the upper continental crust, *Geofluids*, *10*(1□2), 241-253.

Chipera, S. J., and J. A. Apps (2001), Geochemical stability of natural zeolites, *Reviews in mineralogy and geochemistry*, *45*(1), 117-161.

Clarke, H., L. Eisner, P. Styles, and P. Turner (2014), Felt seismicity associated with shale gas hydraulic fracturing: The first documented example in Europe, *Geophysical Research Letters*, *41*(23), 8308-8314.

Coombs, D. S., et al. (1997), Recommended nomenclature for zeolite minerals; report of the Subcommittee on Zeolites of the International Mineralogical Association, Commission on New Minerals and Mineral Names, *The Canadian Mineralogist*, *35*(6), 1571-1606.

Crossey, L. J., B. R. Frost, and R. C. Surdam (1984), Secondary Porosity in Laumontite-Bearing Sandstones: Part 2. Aspects of Porosity Modification.

Denison, R. E. (1981), Basement rocks in northeastern Oklahoma.

Dick, J. M. (2008), Calculation of the relative metastabilities of proteins using the CHNOSZ software package, *Geochem T*, *9*(10), doi:Artn 10
Doi 10.1186/1467-4866-9-10.

Diehl, T., T. Kraft, E. Kissling, and S. Wiemer (2017), The induced earthquake sequence related to the St. Gallen deep geothermal project (Switzerland): Fault reactivation and fluid interactions imaged by microseismicity, *Journal of Geophysical Research: Solid Earth*, *122*(9), 7272-7290.

Ellsworth, W. L. (2013), Injection-induced earthquakes, *Science*, *341*(6142), 1225942.

Erzinger, J., and I. Stober (2005), Introduction to Special Issue: long□term fluid production in the KTB pilot hole, Germany, *Geofluids*, *5*(1), 1-7.

Evans, D. M. (1966), The Denver area earthquakes and the Rocky Mountain Arsenal disposal well, *The Mountain Geologist*.

Evans, J. P., and F. M. Chester (1995), Fluid□rock interaction in faults of the San Andreas system: Inferences from San Gabriel fault rock geochemistry and microstructures, *Journal of Geophysical Research: Solid Earth*, *100*(B7), 13007-13020.

French, M. E., and W. Zhu (2017), Slow fault propagation in serpentinite under conditions of high pore fluid pressure, *Earth and Planetary Science Letters*, *473*, 131-140.

Friberg, P. A., G. M. Besana□Ostman, and I. Dricker (2014), Characterization of an earthquake sequence triggered by hydraulic fracturing in Harrison County, Ohio, *Seismological Research Letters*, *85*(6), 1295-1307.

Fridriksson, T., D. L. Bish, and D. K. Bird (2003), Hydrogen-bonded water in laumontite I: X-ray powder diffraction study of water site occupancy and structural changes in laumontite during room-temperature isothermal hydration/dehydration, *Am Mineral*, *88*(2-3), 277-287.

Gascoyne, M., and D. Kamineni (1994), The hydrogeochemistry of fractured plutonic rocks in the Canadian Shield, *Applied Hydrogeology*, *2*(2), 43-49.

Goebel, T., S. Hosseini, F. Cappa, E. Hauksson, J. Ampuero, F. Aminzadeh, and J. Saleeby (2016), Wastewater disposal and earthquake swarm activity at the southern end of the Central Valley, California, *Geophysical Research Letters*, *43*(3), 1092-1099.

Goebel, T., M. Weingarten, X. Chen, J. Haffener, and E. Brodsky (2017), The 2016 Mw5. 1 Fairview, Oklahoma earthquakes: Evidence for long-range poroelastic triggering at> 40 km from fluid disposal wells, *Earth and Planetary Science Letters*, *472*, 50-61.

Gottardi, G., and E. Galli (1985), Zeolites of the heulandite group, in *Natural Zeolites*, edited, pp. 256-305, Springer.
Gregory, K. B., R. D. Vidic, and D. A. Dzombak (2011), Water management challenges associated with the production of shale gas by hydraulic fracturing, *Elements*, *7*(3), 181-186.
Hacker, B. R. (1997), Diagenesis and fault valve seismicity of crustal faults, *Journal of Geophysical Research: Solid Earth*, *102*(B11), 24459-24467.
Häring, M. O., U. Schanz, F. Ladner, and B. C. Dyer (2008), Characterisation of the Basel 1 enhanced geothermal system, *Geothermics*, *37*(5), 469-495.
Hay, R. L. (1966), *Zeolites and zeolitic reactions in sedimentary rocks*, Geological Society of America.
Healy, J. H., W. W. Rubey, D. T. Griggs, and C. B. Raleigh (1968), The Denver EarthquakeS, *Science*, *161*(3848), 1301-1310, doi:10.1126/science.161.3848.1301.
Helmold, K. P., and P. C. van de Kamp (1984), Diagenetic Mineralogy and Controls on Albitization and Laumontite Formation in Paleogene Arkoses, Santa Ynez Mountains, California: Part 2. Aspects of Porosity Modification.
Holland, A. A. (2013), Earthquakes triggered by hydraulic fracturing in south□central Oklahoma, *Bulletin of the Seismological Society of America*, *103*(3), 1784-1792.
Horálek, J., Z. Jechumtálová, L. Dorbath, and J. Šílený (2010), Source mechanisms of micro-earthquakes induced in a fluid injection experiment at the HDR site Soultz-sous-Forêts (Alsace) in 2003 and their temporal and spatial variations, *Geophysical Journal International*, *181*(3), 1547-1565.
Ikari, M. J., C. Marone, and D. M. Saffer (2011), On the relation between fault strength and frictional stability, *Geology*, *39*(1), 83-86.
Ivanov, I., and L. Gurevich (1975), Experimental study of T-XCO2 boundaries of metamorphic zeolite facies, *Contributions to Mineralogy and Petrology*, *53*(1), 55-60.
Jahr, T., G. Jentzsch, A. Gebauer, and T. Lau (2008), Deformation, seismicity, and fluids: Results of the 2004/2005 water injection experiment at the KTB/Germany, *Journal of Geophysical Research: Solid Earth*, *113*(B11).
Jove, C., and B. R. Hacker (1997), Experimental investigation of laumontite→ wairakite+ H2O: A model diagenetic reaction, *American Mineralogist*, *82*(7-8), 781-789.
Keranen, K. M., H. M. Savage, G. A. Abers, and E. S. Cochran (2013), Potentially induced earthquakes in Oklahoma, USA: Links between wastewater injection and the 2011 Mw 5.7 earthquake sequence, *Geology*, *41*(6), 699-702.
Keranen, K. M., M. Weingarten, G. A. Abers, B. A. Bekins, and S. Ge (2014), Sharp increase in central Oklahoma seismicity since 2008 induced by massive wastewater injection, *Science*, *345*(6195), 448-451.
Kim, W. Y. (2013), Induced seismicity associated with fluid injection into a deep well in Youngstown, Ohio, *Journal of Geophysical Research: Solid Earth*, *118*(7), 3506-3518.
Ko, S. c., D. L. Olgaard, and U. Briegel (1995), The transition from weakening to strengthening in dehydrating gypsum: Evolution of excess pore pressures, *Geophysical Research Letters*, *22*(9), 1009-1012.
Ko, S. C., D. L. Olgaard, and T. F. Wong (1997), Generation and maintenance of pore pressure excess in a dehydrating system 1. Experimental and microstructural observations, *Journal of Geophysical Research: Solid Earth*, *102*(B1), 825-839.
Leclère, H., D. Faulkner, J. Wheeler, and E. Mariani (2016), Permeability control on transient slip weakening during gypsum dehydration: Implications for earthquakes in subduction zones, *Earth and Planetary Science Letters*, *442*, 1-12.
Lester, Y., I. Ferrer, E. M. Thurman, K. A. Sitterley, J. A. Korak, G. Aiken, and K. G. Linden (2015), Characterization of hydraulic fracturing flowback water in Colorado: Implications for water treatment, *Science of the Total Environment*, *512*, 637-644.
Liou, J. (1971), P—T Stabilities of Laumontite, Wairakite, Lawsonite, and Related Minerals in the System CaAl2Si2O8-SiO2-H2O, *Journal of Petrology*, *12*(2), 379-411.
Llana□Fúnez, S., K. Brodie, E. Rutter, and J. Arkwright (2007), Experimental dehydration kinetics of serpentinite using pore volumometry, *Journal of Metamorphic Geology*, *25*(4), 423-438.
Lockner, D. A., C. Morrow, D. Moore, and S. Hickman (2011), Low strength of deep San Andreas fault gouge from SAFOD core, *Nature*, *472*(7341), 82.
Luquot, L., M. Andreani, P. Gouze, and P. Camps (2012), CO 2 percolation experiment through chlorite/zeolite-rich sandstone (Pretty Hill Formation–Otway Basin–Australia), *Chemical geology*, *294*, 75-88.

Malvoisin, B., N. Brantut, and M.-A. Kaczmarek (2017), Control of serpentinisation rate by reaction-induced cracking, *Earth and Planetary Science Letters*, *476*, 143-152.
McCulloh, T. H., V. A. Frizzell, R. J. Stewart, and I. Barnes (1981), Precipitation of laumontite with quartz, thenardite, and gypsum at Sespe Hot Springs, western Transverse Ranges, California, *Clays and Clay Minerals*, *29*(5,353-364).
McMahon, N. D., R. C. Aster, W. L. Yeck, D. E. McNamara, and H. M. Benz (2017), Spatiotemporal evolution of the 2011 Prague, Oklahoma, aftershock sequence revealed using subspace detection and relocation, *Geophysical Research Letters*, *44*(14), 7149-7158.
McNamara, D. E., H. M. Benz, R. B. Herrmann, E. A. Bergman, P. Earle, A. Holland, R. Baldwin, and A. Gassner (2015), Earthquake hypocenters and focal mechanisms in central Oklahoma reveal a complex system of reactivated subsurface strike□slip faulting, *Geophysical Research Letters*, *42*(8), 2742-2749.
Meller, C., and B. Ledésert (2017), Is There a Link Between Mineralogy, Petrophysics, and the Hydraulic and Seismic Behaviors of the Soultz□sous□Forêts Granite During Stimulation? A Review and Reinterpretation of Petro□Hydromechanical Data Toward a Better Understanding of Induced Seismicity and Fluid Flow, *Journal of Geophysical Research: Solid Earth*, *122*(12), 9755-9774.
Miller, S., W. Van Der Zee, D. Olgaard, and J. Connolly (2003), A fluid-pressure feedback model of dehydration reactions: experiments, modelling, and application to subduction zones, *Tectonophysics*, *370*(1-4), 241-251.
Milsch, H., and M. Priegnitz (2012), Evolution of microstructure and elastic wave velocities in dehydrated gypsum samples, *Geophysical Research Letters*, *39*(24).
Mironenko, M., and M. Y. Zolotov (2012), Equilibrium-kinetic model of water-rock interaction, *Geochemistry international*, *50*(1), 1-7.
Moore, D. E., and D. A. Lockner (2007), Friction of the smectite clay montmorillonite, *The seismogenic zone of subduction thrust faults*, 317-345.
Moore, D. E., and D. A. Lockner (2013), Chemical controls on fault behavior: Weakening of serpentinite sheared against quartz□bearing rocks and its significance for fault creep in the San Andreas system, *Journal of Geophysical Research: Solid Earth*, *118*(5), 2558-2570.
Moore, D. E., and M. J. Rymer (2007), Talc-bearing serpentinite and the creeping section of the San Andreas fault, *Nature*, *448*(7155), 795.
Morrow, C. A., D. E. Moore, and D. A. Lockner (2000), The effect of mineral bond strength and adsorbed water on fault gouge frictional strength, *Geophysical research letters*, *27*(6), 815-818.
Morrow, C. A., D. E. Moore, and D. A. Lockner (2017), Frictional strength of wet and dry montmorillonite, *Journal of Geophysical Research: Solid Earth*, *122*(5), 3392-3409.
Neuhoff, P. S., and D. K. Bird (2001), Partial dehydration of laumontite: thermodynamic constraints and petrogenetic implications, in *Mineralogical Magazine*, edited, p. 59, doi:10.1180/002646101550127.
Norbeck, J., and J. Rubinstein (2018), Hydromechanical earthquake nucleation model forecasts onset, peak, and falling rates of induced seismicity in Oklahoma and Kansas, *Geophysical Research Letters*, *45*(7), 2963-2975.
Okazaki, K., and G. Hirth (2016), Dehydration of lawsonite could directly trigger earthquakes in subducting oceanic crust, *Nature*, *530*(7588), 81.
Olgaard, D. L., S.-c. Ko, and T.-f. Wong (1995), Deformation and pore pressure in dehydrating gypsum under transiently drained conditions, *Tectonophysics*, *245*(3-4), 237-248.
Ramudo, A., and S. Murphy (2010), Hydraulic Fracturing–Effects on Water Quality, *Cornell University City and Regional Planning CRP*, *5072*.
Saffer, D. M., D. A. Lockner, and A. McKiernan (2012), Effects of smectite to illite transformation on the frictional strength and sliding stability of intact marine mudstones, *Geophysical Research Letters*, *39*(11).
Savage, D. (1986), Granite-water interactions at 100 C, 50 MPa: an experimental study, *Chemical geology*, *54*(1-2), 81-95.
Savage, D., M. R. Cave, D. Haigh, A. E. Milodowski, and M. E. Young (1993), The reaction kinetics of laumontite under hydrothermal conditions, *European Journal of Mineralogy*, 523-536.
Schleicher, A. M., S. N. Tourscher, B. A. van der Pluijm, and L. N. Warr (2009), Constraints on mineralization, fluid□rock interaction, and mass transfer during faulting at 2–3 km depth from the SAFOD drill hole, *Journal of Geophysical Research: Solid Earth*, *114*(B4).

Schleicher, A. M., L. N. Warr, B. Kober, E. Laverret, and N. Clauer (2006), Episodic mineralization of hydrothermal illite in the Soultz-sous-Forêts granite (Upper Rhine Graben, France), *Contributions to Mineralogy and Petrology*, *152*(3), 349-364.
Scuderi, M., C. Collettini, and C. Marone (2017), Frictional stability and earthquake triggering during fluid pressure stimulation of an experimental fault, *Earth and Planetary Science Letters*, *477*, 84-96.
Shah, A. K., and G. R. Keller (2017), Geologic influence on induced seismicity: Constraints from potential field data in Oklahoma, *Geophysical Research Letters*, *44*(1), 152-161.
Shapiro, S., J. Kummerow, C. Dinske, G. Asch, E. Rothert, J. Erzinger, H. J. Kümpel, and R. Kind (2006), Fluid induced seismicity guided by a continental fault: Injection experiment of 2004/2005 at the German Deep Drilling Site (KTB), *Geophysical Research Letters*, *33*(1).
Shirzaei, M., W. L. Ellsworth, K. F. Tiampo, P. J. González, and M. Manga (2016), Surface uplift and time-dependent seismic hazard due to fluid injection in eastern Texas, *Science*, *353*(6306), 1416-1419.
Skoumal, R. J., M. R. Brudzinski, and B. S. Currie (2015), Earthquakes induced by hydraulic fracturing in Poland Township, Ohio, *Bulletin of the Seismological Society of America*, *105*(1), 189-197.
Solum, J. G., S. H. Hickman, D. A. Lockner, D. E. Moore, B. A. van der Pluijm, A. M. Schleicher, and J. P. Evans (2006), Mineralogical characterization of protolith and fault rocks from the SAFOD main hole, *Geophysical Research Letters*, *33*(21).
Stober, I., and K. Bucher (2005), The upper continental crust, an aquifer and its fluid: hydaulic and chemical data from 4 km depth in fractured crystalline basement rocks at the KTB test site, *Geofluids*, *5*(1), 8-19.
Stober, I., and K. Bucher (2015), Hydraulic conductivity of fractured upper crust: insights from hydraulic tests in boreholes and fluid□rock interaction in crystalline basement rocks, *Geofluids*, *15*(1-2), 161-178.
Tembe, S., D. A. Lockner, and T. F. Wong (2010), Effect of clay content and mineralogy on frictional sliding behavior of simulated gouges: Binary and ternary mixtures of quartz, illite, and montmorillonite, *Journal of Geophysical Research: Solid Earth*, *115*(B3).
Trotignon, L., C. Beaucaire, D. Louvat, and J.-F. Aranyossy (1999), Equilibrium geochemical modelling of Äspö groundwaters: a sensitivity study of thermodynamic equilibrium constants, *Applied geochemistry*, *14*(7), 907-916.
Van der Elst, N. J., H. M. Savage, K. M. Keranen, and G. A. Abers (2013), Enhanced remote earthquake triggering at fluid-injection sites in the midwestern United States, *Science*, *341*(6142), 164-167.
Vincent, M. W., and P. L. Ehlig (1988), Laumontite mineralization in rocks exposed north of San Andreas fault at Cajon Pass, southern California, *Geophysical Research Letters*, *15*(9), 977-980.
Voltolini, M., G. Artioli, and M. Moret (2012), The dissolution of laumontite in acidic aqueous solutions: A controlled-temperature in situ atomic force microscopy study, *American Mineralogist*, *97*(1), 150-158.
Weisenberger, T., and K. Bucher (2010), Zeolites in fissures of granites and gneisses of the Central Alps, *Journal of Metamorphic Geology*, *28*(8), 825-847.
Wong, T. F., S. C. Ko, and D. L. Olgaard (1997), Generation and maintenance of pore pressure excess in a dehydrating system 2. Theoretical analysis, *Journal of Geophysical Research: Solid Earth*, *102*(B1), 841-852.
Zoback, M. D. (2010), *Reservoir geomechanics*, Cambridge University Press.
Zwingmann, H., and N. Mancktelow (2004), Timing of Alpine fault gouges, *Earth and Planetary Science Letters*, *223*(3-4), 415-425.